

Spectroscopy of high spin states in ^{23}Na using the $^{12}\text{C}(^{12}\text{C}, p\gamma)^{23}\text{Na}$ reaction*

G. J. KeKelis,[†] A. H. Lumpkin, K. W. Kemper, and J. D. Fox

Department of Physics, The Florida State University, Tallahassee, Florida 32306

(Received 2 June 1976; revised manuscript received 28 September 1976)

Particle- γ -ray angular correlations have been performed using the $^{12}\text{C}(^{12}\text{C}, p\gamma)^{23}\text{Na}$ reaction at the resonant laboratory energy of 38.82 MeV. Branching ratios, mixing ratios, and lifetimes are determined for the γ decay of states up to 13 MeV excitation energy in ^{23}Na . These results are combined with the $^{12}\text{C}(^{12}\text{C}, ^8\text{Be})^{16}\text{O}$, $^{12}\text{C}(^{12}\text{C}, d)^{22}\text{Na}$, and $^{12}\text{C}(^{12}\text{C}, p)^{23}\text{Na}$ reaction analyses to produce the following spin and parity assignments: 6.114 MeV ($11/2^+$), 6.235 MeV ($13/2^+$), 7.267 MeV ($13/2^+$), 9.038 MeV ($15/2^+$), and 9.803 MeV ($15/2^+$). Shell-model calculations are superior to Nilsson model calculations in describing these results.

NUCLEAR REACTIONS $^{12}\text{C}(^{12}\text{C}, p\gamma)$, $E_{^{12}\text{C}} = 38.82$ MeV, measured lifetimes, branching ratios, and p - γ angular correlations. Deduced J^π of ^{23}Na levels. Compared results with shell and Nilsson models.

I. INTRODUCTION

A large amount of experimental effort is currently directed at identifying selectively populated states at high excitation energies in nuclei. A particularly intriguing case involves the states at 9.04 and 9.80 MeV in ^{23}Na which are strongly populated in the $^{12}\text{C}(^{12}\text{C}, p)$ reaction at $E_{\text{c.m.}} = 19.3$ MeV. Prior to 1973 the spectroscopy on ^{23}Na was limited to states up to about 6.0 MeV in excitation energy; a large number of states were identified up to 10 MeV excitation energy, but definite spin assignments were rare. In 1973 Frank *et al.*¹ used the $^{12}\text{C}(^{12}\text{C}, p\gamma)^{23}\text{Na}$ reaction to selectively populate states up to as high as 10 MeV excitation energy. Using this same reaction, Van Bibber *et al.*² observed anomalous behavior at $E_B = 38.6$ MeV in the population of a number of states at excitation energies between 9.0 and 16.0 MeV. This group³ also postulated that the two strongly enhanced states at 9.0 and 9.8 MeV excitation energy were the $15/2^+$ and $17/2^+$ members of the ground state rotational band. More recent investigations of the $^{12}\text{C}(^{12}\text{C}, p)^{23}\text{Na}$ reaction using the particle- γ -ray angular correlation technique by Green *et al.*,⁴ KeKelis, Lumpkin, and Fox,⁵ and Back *et al.*⁴ Confirmed that these states are of high spin with spin of at least $15/2$. Using the $^{11}\text{B}(^{16}\text{O}, \alpha)^{23}\text{Na}$ reaction and a statistical model analysis of energy averaged data, del Campo *et al.*⁶ have analyzed states up to 15.0 MeV in ^{23}Na and have tentatively identified members of three rotational bands up to $21/2^+$. This work is complemented by the investigation of Gustafson *et al.*⁷ using the $^{12}\text{C}(^{15}\text{N}, \alpha)^{23}\text{Na}$ reaction.

The purpose of the present work is to present the complete results of a $^{12}\text{C}(^{12}\text{C}, p\gamma)^{23}\text{Na}$ reaction study at the resonant incident laboratory energy of $E_B = 38.82$ MeV. States included in this analysis ranged from 2.0 to 16.0 MeV excitation energy in

^{23}Na . Lifetimes of excited states are determined using the Doppler-shift attenuation method (DSAM), and branching ratios and mixing ratios are measured. These results are used to calculate transition strengths, and the above quantities are then compared with both Nilsson and shell-model calculations for ^{23}Na .

II. EXPERIMENTAL PROCEDURE

The $^{12}\text{C}(^{12}\text{C}, p\gamma)^{23}\text{Na}$ measurements to be reported in this work were carried out in a small volume chamber of diameter 12.7 cm. This chamber allowed the Ge(Li) detectors to be placed close to the target. A small diameter (1.27 cm) beam entrance tube allowed Ge(Li) detector angles of 160° with respect to the beam. A $\Delta E \times E$ counter telescope consisting of a $94 \mu\text{m}$ ΔE Si surface barrier detector and a $4000 \mu\text{m}$ Si(Li) E detector cooled to -30°C was positioned at 0° to the beam.

The ^{12}C beam was produced in an inverted sputter source⁸ and accelerated to 38.82 MeV in a 4^+ charge state by the Florida State University super FN tandem Van de Graaff accelerator. This particular beam energy was chosen because states at 14.5 MeV excitation energy in ^{23}Na were more strongly enhanced than at $E_B = 38.6$ MeV. Between 400 and 500 nA of beam were used in this experiment.

The carbon target had to be thin enough to allow the recoiling ions to reach the backing material prior to γ decay, in order that the lifetimes could be measured by DSAM techniques. Since the lifetimes of the excited states of ^{23}Na are typically less than 50 fsec (Ref. 9) and the recoiling ions are confined to a narrow cone around 0° with $v \approx 0.035c$ in this experiment, the target thickness was chosen to be as thin as possible consistent with practical running times. The recoiling ^{23}Na ions require about 25 fsec to traverse the full thickness of the $62 \mu\text{g}/\text{cm}^2$ carbon target which

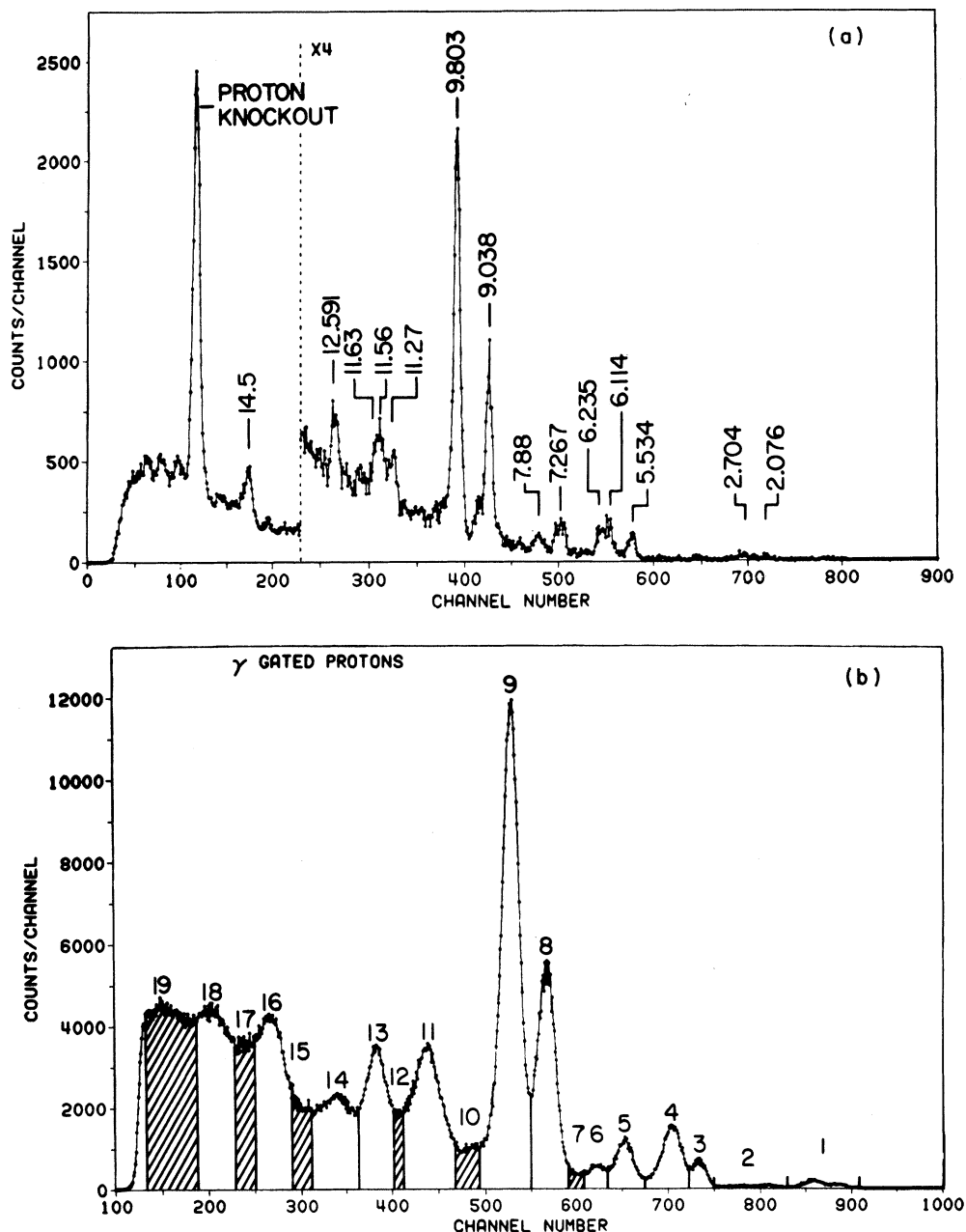


FIG. 1. (a) High resolution proton energy spectrum from the $^{12}\text{C}(^{12}\text{C}, p)^{23}\text{Na}$ reaction at $E_B = 38.8$ MeV and $\theta = 0^\circ$. (b) Coincident proton spectrum showing the various gate regions.

was used in the experiment. The target was made by evaporating carbon onto a 100 mg/cm^2 gold backing which had been cleaned with acetic acid, washed with acetone, and blown dry with dry nitrogen. Care was taken to avoid water contamination since proton knockout at 0° to the beam produced a count rate problem in the particle telescope (see Fig. 1). Another source of background in the particle telescope was the α particles from the $^{12}\text{C}(^{12}\text{C}, \alpha)^{20}\text{Ne}$ reaction. These α particles

were largely eliminated by placing an additional 200 mg/cm^2 of gold absorber directly in front of the particle telescope.

The particle telescope subtended a solid angle of 50 ± 30 msr with an angular acceptance half-angle of $7^\circ \pm 2^\circ$. Three Ge(Li) detectors were used in this experiment. Their volumes were 70, 50, and 40 cm^3 and all had resolutions of 2.5 keV at 1.33 MeV. The γ -radiation pattern was measured at 54° , 70° , 90° , 144° , and 160° to the beam. Data

were taken with each of the two largest detectors at two different angles while the 40 cm³ detector remained stationary at 144° (lab) to act as a monitor.

The short lifetimes of excited states in ²³Na produce severe Doppler effects on the emitted γ radiation in the present experiment. Since Doppler broadening depends on the solid angle subtended by the γ -ray detector, data were taken for several target-detector separations. Data taken for separations of 6 and 15 cm are shown in Fig. 2. The vast improvement in the quality of the data compensates for the decreased count rate obtained at the larger separation distance. During the angular correlation measurements, the front faces of the 70, 50, and 40 cm³ Ge(Li) detectors were placed 18, 15, and 15 cm, respectively, from the target.

Standard electronics were used for this experiment, but high quality spectroscopy amplifiers were necessary to preserve the γ -ray energy resolution when counting at rates in excess of 15 000

counts/sec. Fast timing was performed between the particle E detector and each Ge(Li) detector, with a separate time to amplitude converter (TAC) being used for each Ge(Li) detector. When an event which satisfied the coincidence conditions was detected, the analog to digital converters (ADC) were enabled and signals from the particle detector telescope elements (E and ΔE), the γ -ray-particle time difference (TAC), and the γ -ray energy signal (EGAM) were each digitized in a separate ADC. The three TAC and EGAM signals were multiplexed before entering the ADC and were tagged accordingly. Since each TAC and EGAM signal was separately tagged, the effective "accidental dead time," produced by misidentified events resulting from high counting rates, could be corrected for in the off-line analysis. Resulting four-parameter data were stored in the memory of an on-line EMR 6130 computer in the list mode, then stored on a magnetic disk, and finally, written on magnetic tape.

The natural carbon target thickness of 62 ± 2 $\mu\text{g}/\text{cm}^2$ was determined by comparing the yield of the 9.803 MeV state for the unknown target to the yield of a carbon target whose thickness was determined by comparing low energy proton scattering to the data of Barnard, Swint, and Clegg.¹⁰ This measurement was repeated at the end of the experiment and showed the carbon buildup to be less than 2%. The Ge(Li) detectors were calibrated for relative efficiency using a ⁵⁶Co source which was mounted on a 100 mg/cm² gold backing and placed on the target rod in the same orientation as the target. In this way the relative efficiencies of all three Ge(Li) detectors could be determined without having to make additional absorption corrections. Each detection system was also checked for gain shifts and resolution deterioration as a function of counting rate. Each system retained gain stability to better than two parts in 10 000 up to a counting rate of 15 000 counts/sec, and resolution deteriorated to no more than 9.0 keV for a 3253 keV γ ray at 15 000 counts/sec. These measurements were also repeated at the end of the run. The entire detection system efficiency was measured by placing the Ge(Li) detectors at symmetric angles on opposite sides of the beam line and accumulating on-line data. This was an important measurement since it was the only way to check the counting efficiency of the electronics. Two methods were used to normalize the two sets of particle- γ -ray angular correlation data. First, the beam integration on the target rod and second, the 144° Ge(Li) detector which remained stationary as a monitor throughout the experiment. The two methods agreed to within 1%. During the run 50 mC of charge was

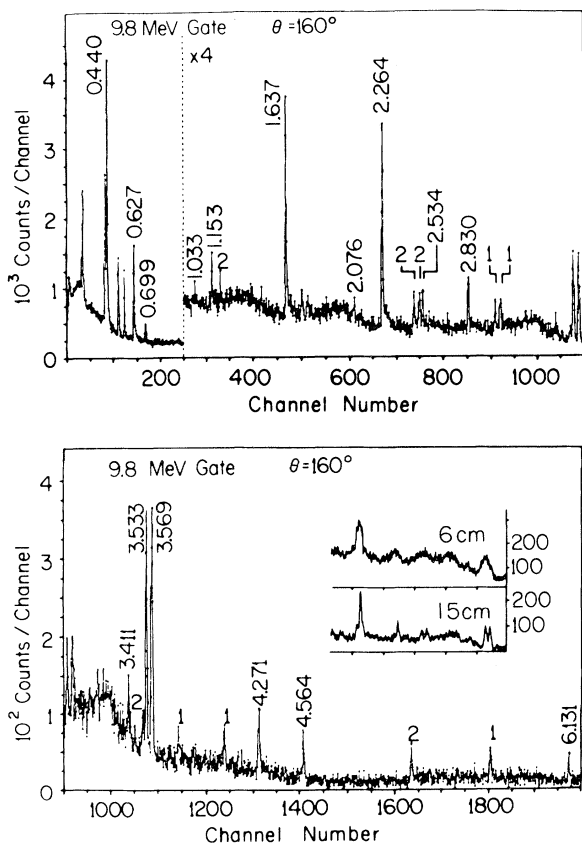


FIG. 2. γ -ray energy spectrum taken at 160° to the beam and gated on the 9.8 MeV excitation region in ²³Na. First and second escape peaks are marked 1 and 2, respectively. The inset illustrates the effect of target-to-Ge(Li) detector distance on Doppler broadening.

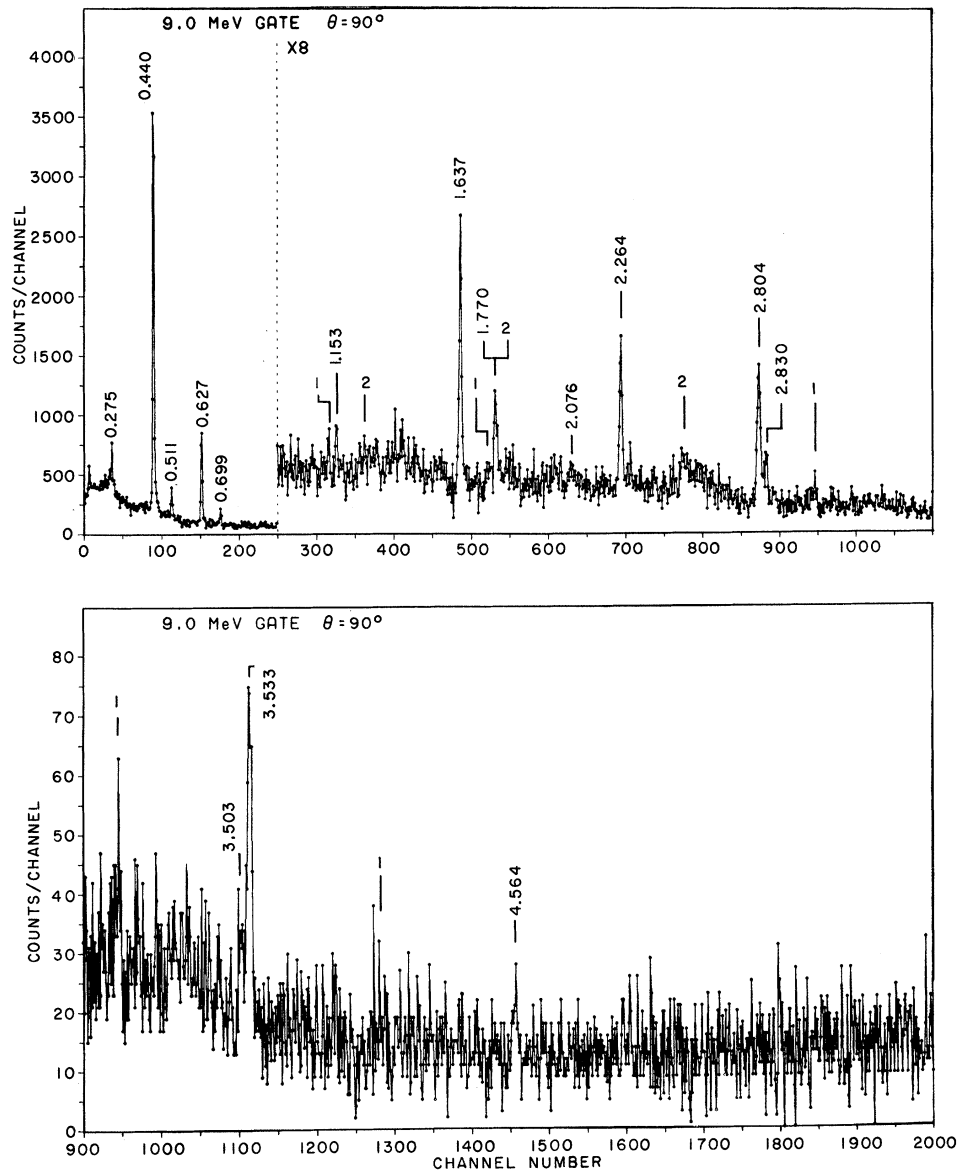


FIG. 3. γ -ray energy spectrum taken at 90° to the beam and gated on the 9.0 MeV excitation region in ^{23}Na . First and second escape peaks are marked 1 and 2, respectively.

collected at each angle setting and 14 million coincidences were detected.

III. DATA AND ANALYSIS

The multiparameter data were sorted off line to generate the proton-gated γ -ray spectra of interest. The windows set on the proton groups for the analysis are shown in Fig. 1(b). The cross-hatched areas are regions of the continuum that were also used as gates. A higher resolution proton spectrum is also shown in Fig. 1(a) which gives the excitation energies for states in ^{23}Na populated by the various proton groups. Accidental coincidences

were subtracted during the analysis to produce the final γ -ray spectra shown in Figs. 3–5 which were gated by the $E_p = 9.0, 9.8,$ and 12.5 MeV regions, respectively. The γ rays are labeled by their unshifted energies. Note that Figs. 3 and 4 show data that were taken at 90° and, although the γ -ray intensities typical of quadrupole transitions are a minimum at this angle and the Doppler-broadening is a maximum, key γ rays are resolved.

γ peak shapes in these spectra are a function of the γ -ray energy, the detection angle, and the lifetime of the state emitting the radiation. Because of this shape effect, peak yields were de-

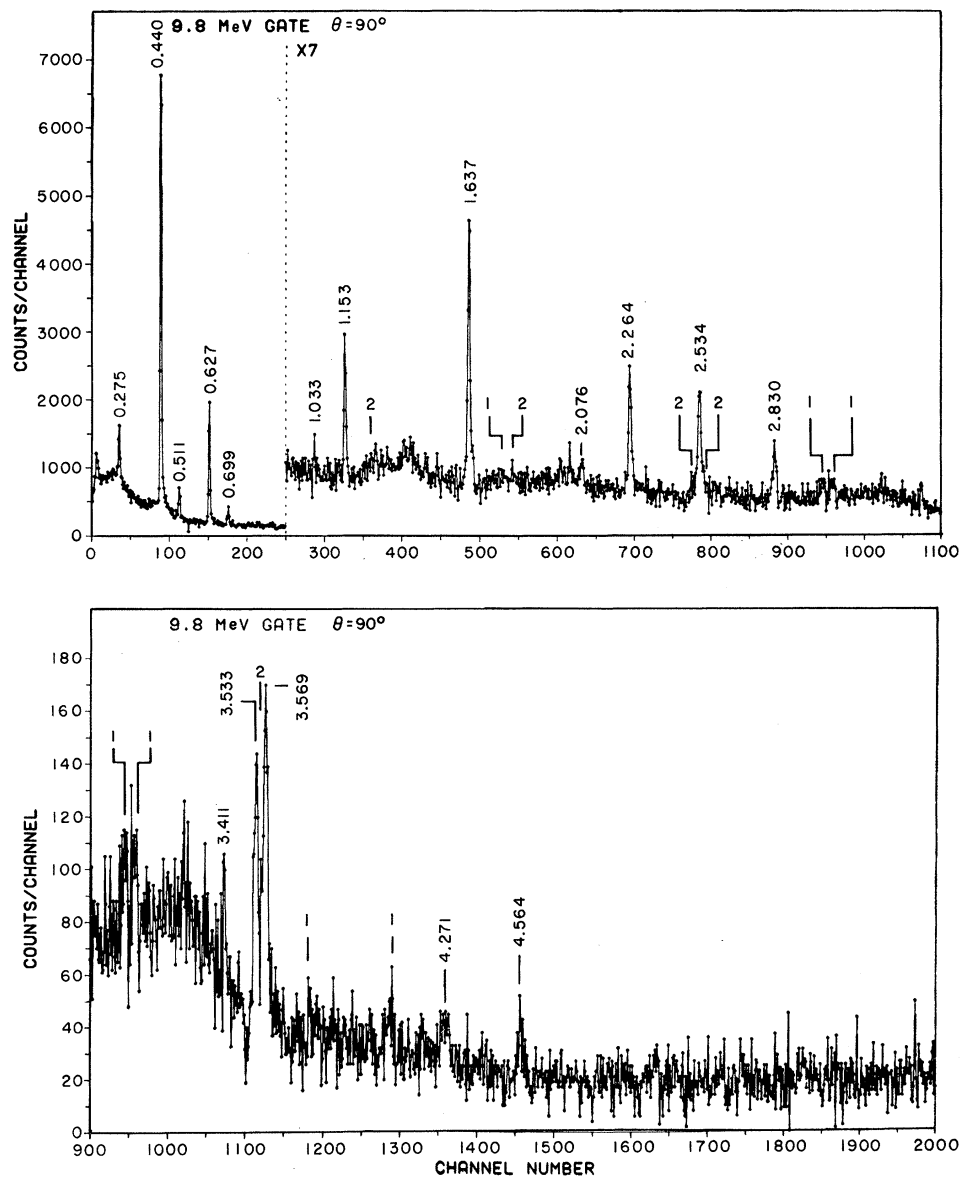


FIG. 4. γ -ray energy spectrum taken at 90° to the beam and gated on the 9.8 MeV excitation region in ^{23}Na . First and second escape peaks are marked 1 and 2, respectively.

terminated by adding the experimental data points and subtracting a linear background. For close lying doublets, this procedure was checked by fitting the peaks to a Gaussian shape. A number of peak yields were complicated by first and second escape peaks from higher energy γ rays and yields were corrected for their presence. Centroids were determined with a first moment calculation.

The particle- γ -ray angular correlations were performed in the "method II" geometry of Litherland and Ferguson¹¹ with the emitted proton detected at 0° to the beam. In the present experi-

ment the proton is detected in an angular range of $\pm 7^\circ$ about the beam axis. To determine how much the complete alignment is disturbed by this finite angular acceptance, transmission coefficients were calculated for 18 MeV protons incident on ^{23}Na . This is the energy of protons leading to the 9.038 MeV state in ^{23}Na produced from the $^{12}\text{C}(^{12}\text{C}, p)^{23}\text{Na}$ reaction at $E_{c.m.} = 19.4$ MeV. The calculation indicates that for an angle of $\pm 10^\circ$, the proton has a maximum projection of orbital angular momentum along the beam axis of $0.7\hbar$; therefore, only the $\pm \frac{1}{2}$ magnetic substates were considered in the analyses of this experiment.

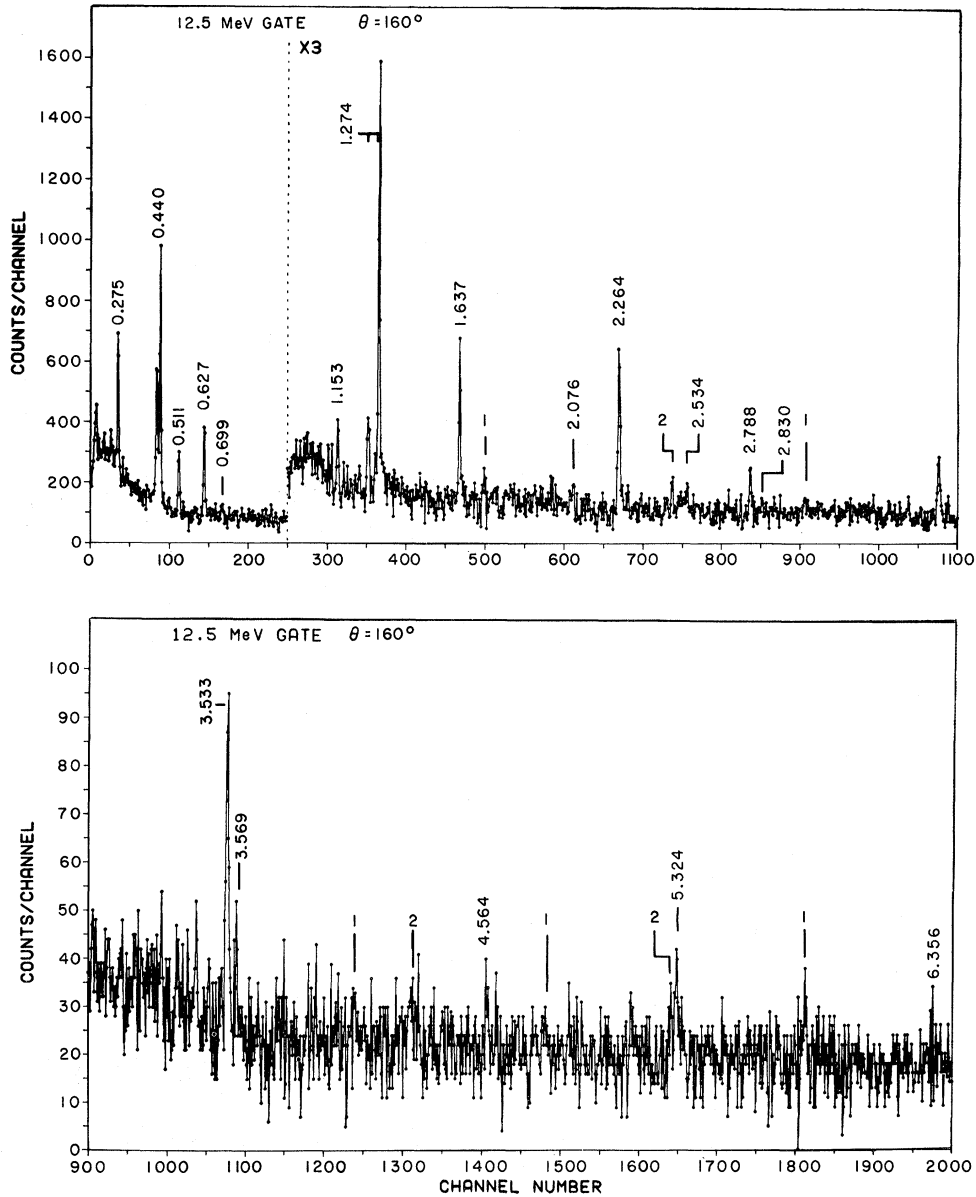


FIG. 5. γ -ray energy spectrum taken at 160° to the beam and gated on the 12.5 MeV excitation region in ^{23}Na . The 1.27 MeV γ ray is from neutron emission to states in ^{22}Na . First and second escape peaks are marked 1 and 2, respectively.

The resultant angular correlations for completely aligned states of half-integral spin are described by the equation

$$W(\theta) = 1 + A_2 P_2(\cos\theta) + A_4 P_4(\cos\theta), \quad (1)$$

where

$$A_k = \frac{1}{1 + \delta^2} [B_k(J_i) F_k(J_f L_1 L_2 J_i) + 2\delta B_k(J_i) F_k(J_f L_1 L_2 J_i) + \delta^2 B_k(J_i) F_k(J_f L_2 L_2 J_i)]. \quad (2)$$

In this equation J_i is the spin of the initial state, J_f is the spin of the final state, L_1 is the lower order, L_2 the higher order of radiation being considered, and B_k is the statistical tensor for the complete alignment. Equation (1) is in the notation of Yamazaki and the B_k and F_k coefficients are tabulated for various spin sequences.¹² In this notation the mixing ratio is given as

$$\delta \equiv \frac{\langle J_f | L_2 | J_i \rangle}{\langle J_f | L_1 | J_i \rangle} \quad (3)$$

and is opposite in sign to that of Rose and Brink.¹³

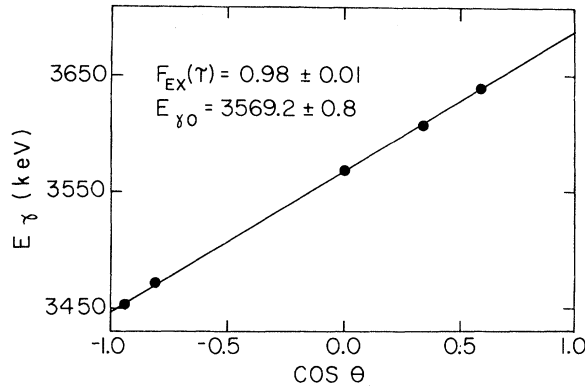


FIG. 6. Plot of the Doppler-shifted γ -ray energy from the 9803 \rightarrow 6235 keV transition as a function of $\cos(\theta)$. The error bars are smaller than the data points.

However, in the following analysis the phase convention will be that of Rose and Brink.

Experimental angular distributions of γ rays were fitted with even order Legendre polynomials up to, and including, $l=4$ with the method of least squares. Mixing ratio calculations were performed for quadrupole and dipole or octupole and quadrupole contributions assuming only population of $\pm\frac{1}{2}$ magnetic substates. Theoretical angular distributions were calculated from Eqs. (1) and (2) assuming a specific spin sequence and mixing ratio. The mixing ratio was then varied from $\theta = -90^\circ$ to $+90^\circ$, where $\theta = \tan^{-1}(\delta)$, and a standard χ^2 analysis was performed between the calculated curve and experimental data for each value of the mixing ratio. A given spin sequence and mixing ratio was considered acceptable if the corresponding reduced χ^2 fell below the 0.1% confidence level.

Experimental values for the Doppler-shift attenuation [$F_{EX}(\tau)$] and the transition energies (E_0)

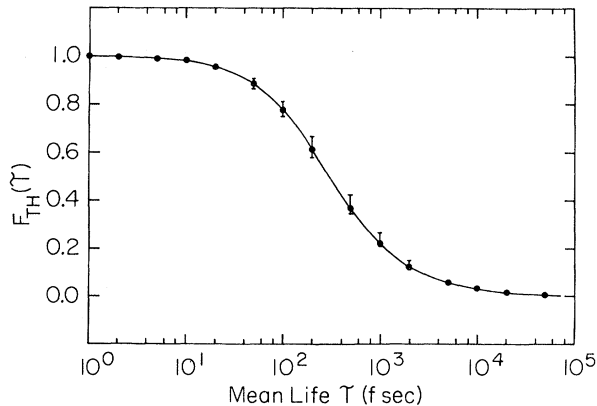


FIG. 7. Theoretical Doppler-shift attenuation function $F_{TH}(\tau)$.

were calculated from the expression

$$E = E_0 [1 + \beta_0 F_{EX}(\tau) \cos(\theta)] \quad (4)$$

by the method of least squares. A plot of the data for the 3569 keV transition is shown in Fig. 6. Theoretical values of $F_{TH}(\tau)$ were calculated for ^{23}Na ions slowing down in layers of carbon and gold, averaged over the thickness of the carbon, using the theory of Blaugrund¹⁴ with atomic stopping powers of Lindhard *et al.*^{15,16} and electron stopping powers from the semiempirical compilation of Northcliffe and Schilling¹⁷ using a version of the Oxford program DSAM.¹⁸ A 20% uncertainty in the electronic stopping powers is included in the lifetime errors.

IV. RESULTS

A. Lifetimes

Lifetimes were determined for as many of the observed transitions as possible and the results are presented in Table I. Since the low-lying states were weakly populated in the reaction, their lifetimes were determined by observing the de-excitation γ rays of these states after they were populated by cascading transitions from higher-lying states. Therefore, the lifetimes measured for the 0.440, 2.076, and 2.704 MeV states determined in the present experiment include the average time required to cascade from states at higher excitation energy. Lifetimes for states above and including the 5.534 MeV state were determined using only γ rays emitted directly from the state of interest. As shown in Table I, previous values were adopted for the 0.440, 2.076, and 2.704 MeV states and an average of present and previous values was adopted for states above and including the 5.534 MeV state. The lifetimes of the 9.038 and 9.803 MeV states were accurately determined in the present experiment. By reducing Doppler effects, as discussed in Sec. II, the key γ rays at 3.569, 2.534, 3.503, and 2.804 MeV were resolved at all angles and additional branches from the 9.0 and 9.8 MeV states were identified. This additional information allowed the γ rays near 3.5 MeV to be corrected for the presence of the second escape peak associated with the 4.564 MeV γ ray (as much as a 10% effect) and allowed multiple measurements for each lifetime. As shown in Table I, an average lifetime was determined when more than one transition was available from a given state. The resulting lifetimes agree well with those determined in previous studies. The lifetime of the 0.440 MeV state was poorly determined because of the small energy shift of this transition. The energy dispersion of the ADC was 3 keV per channel in this work.

TABLE I. Mean lifetimes obtained from the present and previous experiments.

E_x (keV)	Gate E_p (MeV)	E_γ (keV)	$F(\tau)_{\text{exp}}$	τ (fsec)	Average τ (fsec)	Previous τ (fsec)	Adopted (fsec)
440 ^a	2.2 to 12.5	437.8±1.0	0.36±0.10	520±350	520±350	1600±80 ^a	1600±80
2076 ^a	2.2 to 12.5	1635.5±0.8	0.85±0.02	65±25	65±25	40±5 ^a	40±5
2704 ^a	2.2 to 12.5	625.7±0.9	0.86±0.06	61±47	64±22	110±30 ^a	110±30
		2263.1±1.1	0.85±0.02	65±25			
5534±2 ^b	5.5	3457.5±2.5	0.96±0.03	18±18	20±12	12±8 ^c	14±7
	5.5	2829.8±1.2	0.95±0.02	22±15			
6114±2 ^b	6.2	3410.5±1.5	0.91±0.01	39±13	39±13	75±20 ^c	50±11
6235±3 ^b	6.2	699.0±1.4	1.23±0.10	<30	19±18	24±12 ^c	22±10
	6.2	3532.6±2.0	0.96±0.03	19±18			
7267±3 ^b	7.2	1032.6±2.3	0.92±0.10	35±60	26±8	<30 ^c	26±8
	7.2	1153.0±1.0	0.87±0.03	56±28			
	7.2	4563.5±2.0	0.95±0.01	23±9			
9038±5 ^b	9.0	1770.4±1.1	0.97±0.03	15±15	19±10		15±7
	9.0	2803.9±1.2	0.95±0.02	23±14		11±9 ^d	
	9.0	3503.1±3.6	0.96±0.05	19±28		11±9 ^d	
9803±4 ^b	9.8	2534.3±1.4	0.96±0.03	19±18	11±6		11±5
	9.8	3569.2±0.8	0.98±0.01	10±8		12±8 ^d	
	9.8	4270.7±1.5	0.98±0.02	10±10			
12591±5 ^b	12.5	5323.6±1.9	1.03±0.03	<20	<20		<20

^aReference 9.^bPresent experiment.^cReference 1.^dReference 4.

B. Level-energy determinations

The transition energies were determined at the five angles measured and from these transition energies the level energies were determined. Two very accurately known level energies, 2.074 ± 0.0003 and 2.7037 ± 0.0004 MeV, were taken from the literature⁹ and are the reference energies used for determining the energies shown in Table I.

C. Legendre polynomial fits to the angular correlations

The proton gate regions for which angular correlations were analyzed are listed in Table II under the heading Gate. The experimental particle- γ -ray angular correlation data were fit to the expression

$$W(\theta) = a_0 + a_2 P_2(\cos\theta) + a_4 P_4(\cos\theta), \quad (5)$$

where a_0 , a_2 , and a_4 are adjustable coefficients and P_2 and P_4 are Legendre polynomials. The resulting coefficients with $A_2 = a_2/a_0$ and $A_4 = a_4/a_0$ are presented in Table II along with the coefficients from previous studies. A typical angular distribution is shown in Fig. 8.

Transitions proceeding from the 9.038, 9.803, and 12.591 MeV states were analyzed from gate regions which were directly populated by the $^{12}\text{C}(^{12}\text{C}, p)^{23}\text{Na}$ reaction. States at excitation en-

ergies of 7.267, 6.235, and 6.114 MeV were very interesting since the higher-lying states cascaded through them. However, these states were not populated with sufficient strength at the present beam energy to allow all the angular correlations of interest to be directly obtained. Some of the angular correlations for the transitions into and out of these states could only be obtained from gate regions at higher excitation energies, which means that one or even two unobserved transitions preceded the transition of interest. The analysis of angular correlations obtained in this manner did not complicate the procedure of assigning spins and parities because, with the exceptions of the 7.267 to 6.114 and 6.235 to 5.534 MeV transitions, the angular correlations of these transitions did not limit the spins further than those consistent with allowed quadrupole and dipole radiations (see Sec. IV F). However, in order to compare experimental transition strengths with model predictions, experimental mixing ratios must be determined and it is not apparent that valid mixing ratios can be obtained without correcting the angular correlations for the perturbing effects of the unobserved transitions.

As shown by Yamazaki¹² the effect of the unobserved transition is calculable in terms of attenuation coefficients, which multiply the A_2 and A_4 coefficients, if the spin sequence and mixing ratios

TABLE II. Legendre polynomial expansion coefficients as determined in the present and previous experiments.

Transition $E_i(J_i)-E_f(J_f)$	Gate E_p (MeV)	Lindgren	Frank	Green	Present	Present χ^2
		(Ref. 20) A_2 A_4	(Ref. 1) A_2 A_4	(Ref. 4) A_2 A_4	A_2 A_4	
440($\frac{5}{2}^+$)-g.s.($\frac{3}{2}^+$)	2.2 to 12.5	-0.21±0.02 +0.06±0.03			-0.19±0.04 +0.14±0.10	0.9
2 076($\frac{7}{2}^+$)-g.s.($\frac{3}{2}^+$)	2.2 to 12.5 but not 9.8	+0.27±0.08 -0.51±0.12			+0.38±0.15 -0.46±0.27	2.5
2 076($\frac{7}{2}^+$)-440($\frac{5}{2}^+$)	2.2 to 12.5	+0.10±0.02 +0.02±0.03	+0.03±0.03 +0.03±0.03		+0.16±0.04 +0.02±0.07	3.8
2 704($\frac{9}{2}^+$)-440($\frac{5}{2}^+$)	2.2 to 12.5	+0.53±0.10 -0.32±0.17			+0.40±0.04 -0.25±0.07	0.04
2 704($\frac{9}{2}^+$)-2076($\frac{7}{2}^+$)	2.2 to 12.5	-0.14±0.04 +0.10±0.06			-0.18±0.04 -0.01±0.06	0.49
5 534($\frac{11}{2}^+$)-2076($\frac{7}{2}^+$)	5.5	-0.45±0.13 -0.45±0.31	+0.56±0.08 -0.18±0.10		+0.55±0.18 -0.82±0.32	4.1
*5 534($\frac{11}{2}^+$)-2704($\frac{9}{2}^+$)	2.2 to 12.5 but not 9.0	+0.06±0.04 -0.04±0.06	+0.13±0.03 +0.04±0.04		+0.03±0.07 +0.01±0.12	2.27
6 114(-)-2076($\frac{7}{2}^+$)					Not possible	
6 114(-)-2704($\frac{9}{2}^+$)	6.2				+0.15±0.15 +0.39±0.22	1.4
*6 235(-)-2704($\frac{9}{2}^+$)	9.0	+0.20±0.08 -0.38±0.13	+0.44±0.13 -0.16±0.15		+0.39±0.07 -0.24±0.12	2.3
*6 235(-)-2704($\frac{9}{2}^+$)	9.8	+0.20±0.08 -0.38±0.13	+0.44±0.13 -0.16±0.15		+0.44±0.06 -0.19±0.10	2.6
*6 235(-)-5534($\frac{11}{2}^+$)	2.2 to 12.5 but not 9.0				-0.03±0.07 +0.06±0.12	3.1
*7 267(-)-2704($\frac{9}{2}^+$)	7.2+9.0+9.8 +12.5				+0.45±0.11 -0.37±0.19	2.3
*7 267(-)-6114(-)	7.2+9.0+9.8 +11.5+12.5				-0.33±0.07 +0.15±0.10	2.1
7 267(-)-6235($\frac{13}{2}^+$)	7.2				+0.00±0.19 +0.18±0.27	3.2
9 038(-)-5534($\frac{11}{2}^+$)	9.0			+0.44±0.06 -0.23±0.07	+0.06±0.14 -0.50±0.25	2.3
9 038(-)-6235($\frac{13}{2}^+$)	9.0		-0.20±0.07 +0.08±0.08	-0.22±0.04 +0.06±0.04	-0.17±0.05 -0.21±0.08	1.0
9 038(-)-7267(-)	9.0				-0.21±0.10 -0.03±0.15	3.2
9 803(-)-5534($\frac{11}{2}^+$)	9.8				+0.45±0.10 -0.14±0.17	3.5
9 803(-)-6235($\frac{13}{2}^+$)	9.8			+0.40±0.10 -0.04±0.12	+0.23±0.05 +0.08±0.09	2.4
9 803(-)-7267(-)	9.8				-0.39±0.10 -0.34±0.19	0.08
12 591(-)-7267(-)	12.5				+0.04±0.07 -0.32±0.11	2.5

are known. These corrections are not easily incorporated into the analysis of the transitions from the 7.267, 6.235, and 6.144 MeV states since the J^π of at least two of the states in the sequence are unknown. However, corrections were attempted for the 9.803-7.267-6.114 sequence and they did not appreciably affect the resulting mixing ratio for the second transition. This result is partly due to the relatively large errors included in the angular correlations, but it is pre-

dominantly because the unobserved transition does not radically disturb the magnetic substate alignment. Since only the $M_z = \pm \frac{1}{2}$ magnetic substates are populated in this reaction, the attenuation coefficients obtained for an angular correlation of a transition which is preceded by a typical unobserved transition from a state of $\frac{9}{2} \leq J \leq \frac{17}{2}$ are no less than, and probably greater than, $\alpha_2 = 0.88$ and $\alpha_4 = 0.64$. Therefore angular correlation effects persist. To test whether valid mixing ratios

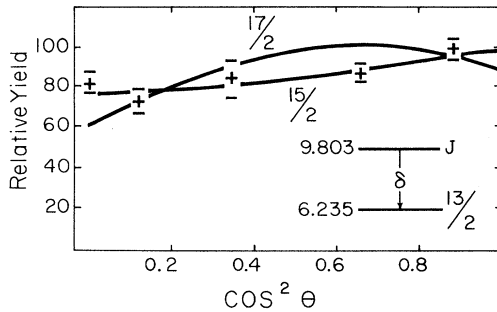


FIG. 8. Angular distribution for the 9803 \rightarrow 6235 keV transition.

could be obtained without making corrections for the expected attenuation, angular correlations were analyzed for transitions from the 5.534, 2.704, 2.076, and 0.440 MeV states which were populated by unobserved cascading transitions from higher lying states. Most of the cascades originated from the 9.038 and 9.803 MeV states since they were populated with the greatest strength. As shown in Table II, the expansion coefficients obtained in this way agree reasonably well, within the experimental errors, with those of previous studies. In addition, as will be discussed in Sec. IV F, the correct transition assignment produced the smallest χ^2 in most cases and, as shown in Table IV, predicted mixing ratios agree with those of previous studies. These results show that reliable spin limitations and mixing ratios can be obtained without making attenuation corrections for two or three unobserved transitions when the first unobserved transition initiates from a highly aligned high spin state. This procedure was used to obtain the experimental mixing ratios shown in Tables IV, VI, and IX with each transition sequence starting from the proton gate regions shown in Table II. Mixing ratios were adopted from previous studies for the transitions from states below 5 MeV, and from the present study for transitions from states above 5 MeV. Those transitions with experimental mixing ratios which are slightly affected by, but not corrected for, the perturbation of an unobserved transition are preceded by an asterisk in Table II.

D. Branching ratios and decay scheme

Because of the superior resolution obtained in the present $^{12}\text{C}(^{12}\text{C}, p\gamma)^{23}\text{Na}$ experiment, a number of new γ -ray decay branches were discovered. The isotropic terms a_0 , resulting from the Legendre polynomial fits to the angular correlation data, were used to calculate branching ratios. These a_0 terms are listed in Table III along with

the calculated branching ratios from the present and previous studies. It is clear from the γ -ray spectra of Figs. 3–5 that weak γ rays are often difficult to observe because of the complexity of the spectra. For these weak γ rays, such as the 1033, 3458, and the 2076 keV γ rays, it was necessary to analyze the γ -ray spectra gated by lower-lying proton groups. The branching ratios given for the 9.803, 9.038, and 7.267 MeV states are those from the present work. For the 6.235 and 5.534 MeV states an average value was adopted using the present and previous values. Since only one branch out of the 6.114 MeV state was strong enough to be analyzed in the present data, the previous results were used for this state. Previous results were also used for the 2.704 and 2.076 MeV states.

The decay scheme which resulted from the analysis of the present data is shown in the energy level diagram of Fig. 9. The intensities of the γ rays participating in the cascades from the 9.038 and 9.803 MeV states were carefully summed to insure that transitions were correctly identified. The total intensity feeding into each state agreed well with the emitted intensity for all but three states. For these three states, at 7.267, 5.534, and 2.076 MeV, from 10 to 25% of the feeding was missing. Also, a total relative intensity of 92.2 ± 3.0 was found to feed the ground state, whereas an intensity of only 73.1 ± 1.6 was emitted from the 9.803 MeV state. The missing intensity is probably due to weak γ -ray branches from the 9.803 MeV gate region which were not identified in the present data. One new branch was detected out of the 9.038 MeV state and two new branches from the 9.803 MeV state. These branches were not detected in other studies of this reaction presumably because of prohibitive Doppler-broadening effects.^{1,3,4}

E. Mixing ratios and transition strength

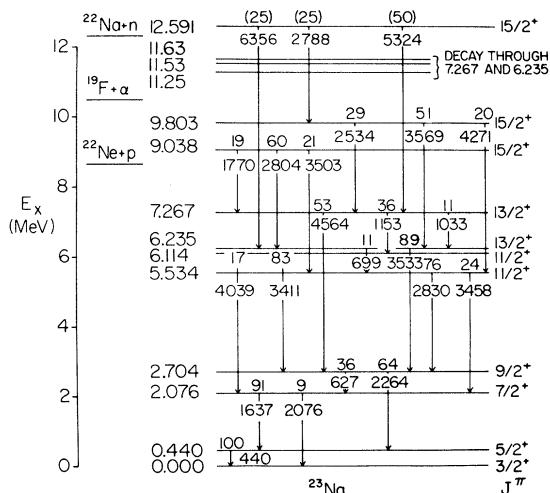
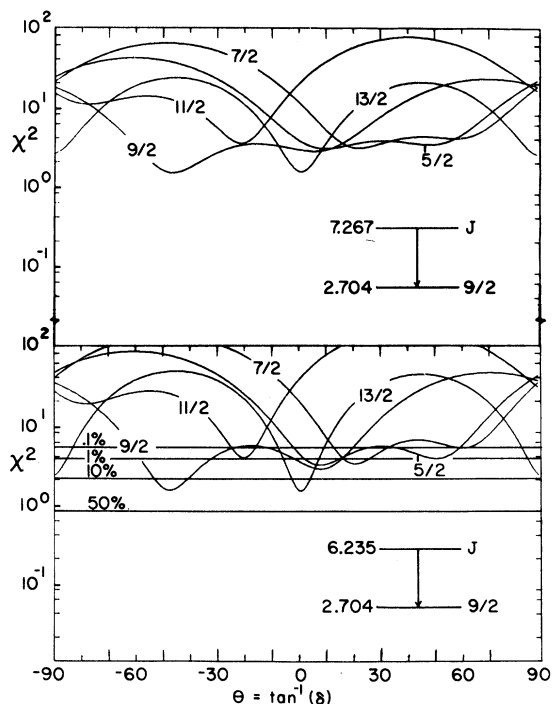
Mixing ratios were calculated as described in Sec. III. Various proton-gated γ -ray spectra were analyzed either separately or in combination to obtain the best possible statistics for each γ ray of interest, and to eliminate complicating Compton edges and first and second escape peaks. For transitions with $|\Delta J| \leq 1$ the mixing ratio involves only quadrupole and dipole contributions and for $|\Delta J| \geq 2$ only octupole and quadrupole contributions. Higher order contributions were not considered since only one $E4$ transition has been detected in the $A = 21$ –44 mass region.¹⁹ A mixing ratio was considered acceptable if a reduced χ^2 of less than 5.5 (0.1% confidence level) was obtained. For a number of transitions, such as those populating the 6.114, 6.235, and 7.267 MeV

TABLE III. Branching ratios (BR) as obtained in the present and previous experiments.

E_i (keV)	E_f (keV)	Gate E_p (MeV)	a_0	Norm. factor	Intensity	Present BR (%)	Previous BR (%)	Adopted BR (%)
2 076	g.s.	2.2 to 12.5	65 ± 2	3.643	17.7 ± 0.5	15 ± 4	9 ± 1^a	9 ± 1
	440	2.2 to 12.5	89 ± 2	0.858	103.5 ± 2.0	85 ± 4	91 ± 1^a	91 ± 1
2 704	440	9.0	80 ± 2	3.318	24.1 ± 0.6	63 ± 3	64 ± 1^a	64 ± 1
	2076	9.0	82 ± 2	5.734	14.3 ± 0.4	37 ± 3	36 ± 1^a	36 ± 1
5 534	2076	5.5	63 ± 6	42.32	1.49 ± 0.13	28 ± 6	24 ± 5^a	26 ± 5
	2704	5.5	95 ± 5	24.19	3.92 ± 0.20	72 ± 6	76 ± 5^a	74 ± 5
6 114	2076						17 ± 4^b	17 ± 4
	2704						83 ± 4^b	83 ± 4
6 235	2704	9.0	76 ± 2	3.851	19.7 ± 0.5	88 ± 5		
	2704	9.8	64 ± 2	1.907	33.6 ± 0.9	84 ± 5	92 ± 5^b	89 ± 5
	5534	9.0	87 ± 3	32.577	2.7 ± 0.1	12 ± 5		
	5534	9.8	88 ± 2	13.379	6.6 ± 0.2	16 ± 5	8 ± 5^b	11 ± 5
7 267	2704	7.2	63 ± 4	18.5	3.41 ± 0.24	53 ± 5		53 ± 5
	6114	7.2	76 ± 3	37.9	2.01 ± 0.08	36 ± 3		36 ± 3
	6235	7.2	62 ± 4	82.9	0.74 ± 0.04	11 ± 2		11 ± 2
9 038	5534	9.0	70 ± 3	8.915	7.9 ± 0.3	21 ± 2	27 ± 5^c	21 ± 2
	6235	9.0	89 ± 2	3.978	22.4 ± 0.5	60 ± 3	73 ± 5^c	60 ± 3
	7267	9.0	78 ± 3	10.752	7.3 ± 0.3	19 ± 2		19 ± 2
9 803	5534	9.8	84 ± 3	5.651	14.9 ± 0.5	20 ± 2		20 ± 2
	6235	9.8	81 ± 2	2.191	37.0 ± 0.5	51 ± 2	100^c	51 ± 2
	7267	9.8	67 ± 2	3.154	21.2 ± 0.5	29 ± 2		29 ± 2
12 591	6235	12.5				(25)		
	7267	12.5				(50)		
	9803	12.5				(25)		

^aReference 9.^bReference 1.^cReference 4.

states, the spin of the final state was not known. Mixing ratio calculations were therefore performed for all reasonable spin combinations and were found to be relatively insensitive to the spin of the final state. Some of the results of these calculations are shown in graphical form in Figs.

FIG. 9. Partial decay scheme of ^{23}Na including the results of the present work.FIG. 10. Mixing ratio calculations for the 7267 \rightarrow 2704 and 6235 \rightarrow 2704 keV transitions.

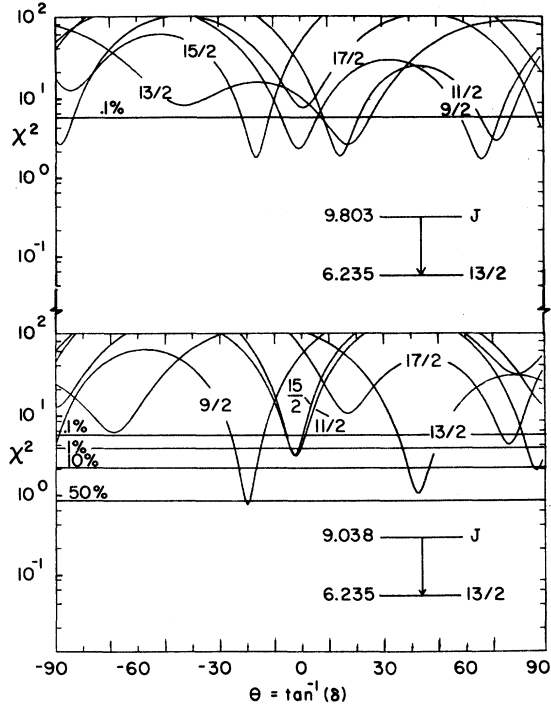


FIG. 11. Mixing ratio calculations for the 9038 → 6235 and 9803 → 6235 keV transitions.

10 and 11. Transition strengths were calculated for each acceptable mixing ratio for both parity change and nonparity change transitions using the adopted values of the lifetimes, branching ratios, and state energies in Tables I and III. Those transition strengths which exceeded the limits $E1 \leq 0.03$, $E2 \leq 100$, $E3 \leq 100$, $M1 \leq 10$, and $M2 \leq 3$ W.u. (Weisskopf units) were considered to be unacceptably large and were eliminated.¹⁹ Although the complete list of calculated transition strengths is too lengthy to be presented, the important values of mixing ratios and reduced transition probabilities are given in Tables IV–VI.

F. Discussion of spin parity assignments

Analysis of the transition strengths calculated in the previous section indicated that the $M2$ transition strengths for parity change transitions ($\delta = M2/E1$) were in general 10 to 100 times greater than the corresponding $E2$ transition strengths ($\delta = E2/M1$). Most of these parity change transitions were eliminated because of unreasonably high implied $M2$ strengths. In addition, only five $M2$ transitions have been identified in this region¹⁹ and no known negative parity states were populated with appreciable strength in this reaction. It is therefore assumed that only positive parity states are being populated and that only nonparity change

TABLE IV. Comparison of present mixing ratios to previous values.

Transition	$J_i \rightarrow J_f$	Previous δ	Present δ	Adopted δ
440-g.s.	$\frac{5}{2} \rightarrow \frac{3}{2}$	-0.057 ± 0.004^a	-0.12 ± 0.05	-0.057 ± 0.004
2076-g.s.	$\frac{7}{2} \rightarrow \frac{3}{2}$	$+0.14 \pm 0.11^a$	$+0.08 \pm 0.37$	$+0.14 \pm 0.11$
2076-440	$\frac{7}{2} \rightarrow \frac{5}{2}$	-0.19 ± 0.02^a	-0.25 ± 0.06	-0.19 ± 0.02
2704-440	$\frac{9}{2} \rightarrow \frac{5}{2}$	$+0.00 \pm 0.03^a$	$+0.02 \pm 0.09$	$+0.00 \pm 0.03$
2704-2076	$\frac{9}{2} \rightarrow \frac{7}{2}$	-0.08 ± 0.02^a	-0.07 ± 0.05	-0.08 ± 0.02
5534-2076	$\frac{11}{2} \rightarrow \frac{7}{2}$	$+0.06 \pm 0.20^b$	$+0.10 \pm 0.30$	$+0.08 \pm 0.25$
5534-2704	$\frac{11}{2} \rightarrow \frac{9}{2}$	-0.17 ± 0.03^b	-0.17 ± 0.11	-0.17 ± 0.03
6235-2704	$\frac{13}{2} \rightarrow \frac{9}{2}$	$+0.15 \pm 0.14^b$	$+0.03 \pm 0.15$	$+0.09 \pm 0.15$
6114-2704	$\frac{9}{2}$	-1.60 ± 0.50^b	-1.05 ± 0.70	-1.32 ± 0.60
	$\frac{11}{2} \rightarrow \frac{9}{2}$	-0.26 ± 0.11^c	-0.26 ± 0.33	
	$\frac{9}{2}$	-1.4 ± 0.5^c	-1.09 ± 0.90	
	$\frac{9}{2}$	$+0.34 \pm 0.17^c$	$+0.29 \pm 0.57$	
	$\frac{7}{2}$	$>0.12^c$	$+0.24 \pm 0.45$	
	$\frac{5}{2}$	$E2^c$	$+0.009 \pm 0.48$	

^aReference 9.

^bReference 20.

^cReference 1.

TABLE V. Shell-model reduced transition probabilities as compared with the experimental values. Experimental transition strengths were obtained using the experimental values of δ , τ , and BR shown in Table VI when that data were available. Theoretical reduced transition probabilities are from Wildenthal and Chung (Ref. 30).

E_i (keV)	J_i	E_f (keV)	J_f	$B(M1)$ (μ_N)		$B(E2)$ ($e^2 \text{ fm}^4$)	
				Exp.	Theory	Exp.	Theory
440	$\frac{5}{2}^+$	0	$\frac{3}{2}^+$	0.41 ± 0.02	0.351	101 ± 15	104.0
2076	$\frac{7}{2}^+$	0	$\frac{3}{2}^+$			47 ± 8	36.8
		440	$\frac{5}{2}^+$	0.28 ± 0.04	0.267	55 ± 14	55.6
2393	$\frac{1}{2}^+$	0	$\frac{3}{2}^+$	$<0.004^a$	0.130	$<8.0^a$	6.15
		440	$\frac{5}{2}^+$			11.6 ± 1.6	13.9
2704	$\frac{9}{2}^+$	440	$\frac{5}{2}^+$			80 ± 22	54.6
		2076	$\frac{7}{2}^+$	0.75 ± 0.21	0.632	175 ± 100	46.0
2984	$\frac{3}{2}^+$	0	$\frac{3}{2}^+$	0.25 ± 0.05	0.519	0.04 ± 0.16	10.8
		440	$\frac{5}{2}^+$	0.29 ± 0.06	0.748	5.18 ± 3.6	2.99
3916	$\frac{5}{2}^+$	0	$\frac{3}{2}^+$	0.074 ± 0.015	0.081	3.36 ± 1.14	0.880
		440	$\frac{5}{2}^+$	$<0.008^a$	0.068	$<13.2^a$	2.36
4430	$\frac{1}{2}^+$	0	$\frac{3}{2}^+$	$<2.54^a$	2.16	$<1600^a$	0.248
		2393	$\frac{1}{2}^+$	1.49 ± 0.53^a	1.58		
4775	$\frac{7}{2}^+$	440	$\frac{5}{2}^+$	0.203 ± 0.102	0.259	4.51 ± 2.50	5.04
		2076	$\frac{7}{2}^+$	0.388 ± 0.200	0.628	1.23 ± 6.50	3.04
		2704	$\frac{9}{2}^+$		0.438		3.10
5374	$\frac{5}{2}^+$	0	$\frac{3}{2}^+$	0.120 ± 0.070	0.176	0.160 ± 0.33	1.82
		440	$\frac{5}{2}^+$	0.71 ± 0.39	1.12	30.8 ± 20.2	1.44
		2076	$\frac{7}{2}^+$	1.12 ± 0.61	1.11	33.6 ± 40.2	1.14
		2984	$\frac{3}{2}^+$		0.676		5.64
5534	$\frac{11}{2}^+$	2076	$\frac{7}{2}^+$			30.6 ± 16.4	56.2
		2704	$\frac{9}{2}^+$	0.13 ± 0.07	0.365	6.7 ± 4.1	24.3
6114	$\frac{11}{2}^+$	2076	$\frac{7}{2}^+$				0.740
		2704	$\frac{9}{2}^+$	0.022 ± 0.006	0.023	$1.87^{+5.9}_{-3.6}$	1.32
6235	$\frac{13}{2}^+$	2704	$\frac{9}{2}^+$			60 ± 27	38.7
		5534	$\frac{11}{2}^+$	0.81 ± 0.53	0.713	471 ± 800	12.8
7267	$\frac{13}{2}^+$	2704	$\frac{9}{2}^+$			8.4 ± 2.7	13.6
		5534	$\frac{11}{2}^+$		0.065		4.58
		6235	$\frac{13}{2}^+$	$0.16^{+0.12}_{-0.52}$	0.187	700^{+9000}_{-2000}	20.9
		6114	$\frac{11}{2}^+$	0.51 ± 0.16	0.453	0.56 ± 10.0	33.5
9038	$\frac{15}{2}^+$	5534	$\frac{11}{2}^+$			$20.2^{+19.2}_{-12.2}$	35.5
		6235	$\frac{13}{2}^+$	0.10 ± 0.05	0.418	0.17 ± 0.57	0.313
		7267	$\frac{13}{2}^+$	0.129 ± 0.062	0.086	0.95 ± 6.7	25.5
9803	$\frac{15}{2}^+$	5534	$\frac{11}{2}^+$			10.47 ± 4.87	12.2
		6235	$\frac{13}{2}^+$	0.054 ± 0.025	0.102	4.76 ± 4.04	25.4
		6114	$\frac{11}{2}^+$				7.09
		7267	$\frac{13}{2}^+$	0.091 ± 0.042	0.304	2.47 ± 6.83	7.20

^aThese experimental values were obtained from Frank *et al.* (Ref. 1).

TABLE VI. Shell-model predictions of mean lifetimes, mixing ratios, and branching ratios (BR) as compared with the experimental values. Theoretical values of τ , BR, and δ were obtained from Ref. 30.

E_i (keV)	J_i	E_f (keV)	J_f	Mixing ratio		Mean life (fs)		Branching ratio (%)	
				Exp.	Theory	Exp.	Theory	Exp.	Theory
440 ^a	$\frac{5}{2}^+$	0	$\frac{3}{2}^+$	-0.057 ± 0.004	-0.063	1600 ± 80	1900.0	100	100.0
2076 ^a	$\frac{7}{2}^+$	0	$\frac{3}{2}^+$	$+0.14 \pm 0.11$		40 ± 5	43.0	9 ± 1	7.6
		440	$\frac{5}{2}^+$	-0.19 ± 0.02	-0.198			91 ± 1	92.4
2393 ^b	$\frac{1}{2}^+$	0	$\frac{3}{2}^+$		+0.137	800 ± 200	31.0	65 ± 1	98.5
		440	$\frac{5}{2}^+$					35 ± 1	1.5
2704 ^a	$\frac{9}{2}^+$	440	$\frac{5}{2}^+$	$+0.00 \pm 0.03$		110 ± 30	152.0	64 ± 1	59.8
		2076	$\frac{7}{2}^+$	-0.08 ± 0.02	-0.044			36 ± 1	40.2
2984 ^b	$\frac{3}{2}^+$	0	$\frac{3}{2}^+$	$+0.01 \pm 0.02$	-0.114	5 ± 1		58 ± 1	53.1
		440	$\frac{5}{2}^+$	$+0.09 \pm 0.03$	-0.042			42 ± 1	46.8
3916 ^b	$\frac{5}{2}^+$	0	$\frac{3}{2}^+$	-0.22 ± 0.03	-0.108	10 ± 2	7.53	82 ± 2	64.9
		440	$\frac{5}{2}^+$		+0.185			8 ± 2	33.2
4430 ^b	$\frac{1}{2}^+$	0	$\frac{3}{2}^+$		+0.013	0.27 ± 0.03	0.28	94 ± 2	92.6
		2393	$\frac{1}{2}^+$					6 ± 2	6.6
4775 ^b	$\frac{7}{2}^+$	440	$\frac{5}{2}^+$	-0.17 ± 0.02	-0.160	<2	1.48	60 ± 3	56.5
		2076	$\frac{7}{2}^+$	$+0.04 \pm 0.10$	-0.050			27 ± 2	32.2
		2704	$\frac{9}{2}^+$		-0.046			13 ± 2	10.3
5374 ^c	$\frac{5}{2}^+$	0	$\frac{3}{2}^+$	$+0.05 \pm 0.05$	+0.145	~ 0.37		13 ± 1	12.9
		440	$\frac{5}{2}^+$	$+0.27 \pm 0.05$	+0.048			60 ± 3	64.1
		2076	$\frac{7}{2}^+$	-0.15 ± 0.08	-0.028			27 ± 3	17.4
		2984	$\frac{3}{2}^+$		-0.062				5.3
5534 ^a	$\frac{11}{2}^+$	2076	$\frac{7}{2}^+$	$+0.08 \pm 0.25$		14 ± 7	5.14	26 ± 5	18.3
		2704	$\frac{9}{2}^+$	-0.17 ± 0.03	-0.196			74 ± 5	81.7
6114 ^a	$\frac{11}{2}^+$	2076	$\frac{7}{2}^+$			50 ± 11	48.9	17 ± 4	5.7
		2704	$\frac{9}{2}^+$	$-0.26^{+0.26}_{-0.41}$	-0.228			83 ± 4	92.8
6235 ^a	$\frac{13}{2}^+$	2704	$\frac{9}{2}^+$	$+0.09 \pm 0.15$		22 ± 10	39.2	89 ± 5	90.9
		5534	$\frac{11}{2}^+$	-0.14 ± 0.11	+0.020			11 ± 5	9.1
7267 ^a	$\frac{13}{2}^+$	2704	$\frac{9}{2}^+$	$+0.03 \pm 0.24$		26 ± 8	19.7	53 ± 5	64.9
		5534	$\frac{11}{2}^+$		+0.118				10.8
		6235	$\frac{13}{2}^+$	$+0.57^{+3.63}_{-0.74}$	+0.098			11 ± 2	8.9
		6114	$\frac{11}{2}^+$	-0.01 ± 0.09	-0.071			36 ± 3	15.3
9038 ^a	$\frac{15}{2}^+$	5534	$\frac{11}{2}^+$	$+0.27^{+0.73}_{-0.32}$		15 ± 7	5.02	21 ± 2	10.2
		6235	$\frac{13}{2}^+$	-0.03 ± 0.05	-0.021			60 ± 3	85.3
		7267	$\frac{13}{2}^+$	-0.04 ± 0.14	+0.250			19 ± 2	4.3
9803 ^a	$\frac{15}{2}^+$	5534	$\frac{11}{2}^+$	-0.03 ± 0.23		11 ± 5	4.73	20 ± 2	8.9
		6235	$\frac{13}{2}^+$	-0.28 ± 0.10	-0.475			51 ± 2	48.4
		6114	$\frac{11}{2}^+$						2.1
		7267	$\frac{13}{2}^+$	$+0.11 \pm 0.15$	+0.101			29 ± 2	39.4

^a Experimental values of τ , BR, and δ obtained from Tables I, III, and IV.^b Experimental values of τ , BR, and δ obtained from Ref. 9.^c Experimental values of τ , BR, and δ obtained from Ref. 32.

transitions occur.

Further analysis of the calculated $M3$ transition strengths indicated that the short lifetimes of the involved states requires the mixing ratio $\delta(M3/E2) \leq 0.05$ to produce a reasonable transition strength. Therefore, the only reasonable $M3$ contribution is almost none at all, and all spin assignments consistent with octupole or higher transitions were excluded from further analysis.

The resulting spin assignments will now be presented.

1. Transitions from the 0.440, 2.076, 2.704, and 5.534 MeV states

The spins and parities of these states have been previously determined.⁹ As discussed in Sec. IV C, the analysis of these low-lying states was included to establish the validity of the present experimental method and analytical techniques. Using only the present data the correct transition assignment produced the smallest χ^2 in all cases except for the 2.704 ($\frac{9}{2}^+$) to 0.440 ($\frac{5}{2}^+$) transition. Also, for each transition the present mixing ratios agree, within the quoted error, with the previous values as shown in Table IV.

2. Transitions from the 6.114 MeV state

The transition from this state to the 2.704 MeV state (83%) agrees with a range of spins from $\frac{5}{2}^+$ to $\frac{13}{2}^+$ for the 6.114 MeV state. The presence of the weak branch (17%) to the $\frac{7}{2}^+$ state at 2.076 MeV eliminates the $\frac{13}{2}^+$ assignment. Consequently, the possible spins for the 6.114 MeV state are $\frac{5}{2}^+$ to $\frac{11}{2}^+$. These results are consistent with the $\frac{5}{2}^+$ to $\frac{11}{2}^+$ limits proposed by Lindgren *et al.*²⁰ They are also consistent with the conclusions of Powers *et al.*^{21,22} which indicated that a doublet of high-spin states was located near 6.115 MeV excitation in ^{23}Na .

3. Transitions from the 6.235 MeV state

The branch from the 6.235 MeV state to the $\frac{11}{2}^+$ state at 5.534 MeV (11%) indicates a $\frac{9}{2}^+$ or $\frac{13}{2}^+$ assignment. As shown in Fig. 10 the main branch (89%) to the $\frac{9}{2}^+$ state at 2.704 MeV implies a range of possible spins from $\frac{5}{2}^+$ to $\frac{13}{2}^+$ with the $\frac{13}{2}^+$ and $\frac{9}{2}^+$ assignments being favored at the 20% confidence level. Therefore, the spin of the 6.235 MeV state is either $\frac{9}{2}^+$ or $\frac{13}{2}^+$. Again, this result is consistent with the $\frac{9}{2}^+$ or $\frac{13}{2}^+$ assignment made by Lindgren *et al.*²⁰ It is important to note that the present analysis of the 6.235 to 5.534 MeV transition indicated a J^π assignment and mixing ratio (Table IV) consistent with those of Lindgren *et al.*,²⁰ even though the transition was not corrected for the presence of unobserved preceding transitions.

4. Transitions from the 7.267 MeV state

The transition to the $\frac{9}{2}^+$ state at 2.704 MeV (53%) did not limit the spin further than the allowed $\frac{5}{2}^+$ to $\frac{13}{2}^+$ values. As shown in Fig. 10, the $\frac{9}{2}^+$ and $\frac{13}{2}^+$ assignments were favored at the 20% confidence level ($\chi^2=1.5$). The strong similarity in the mixing ratio calculations for the decays of the 6.235 and 7.267 MeV states to the 2.704 MeV state probably indicates that these states are of the same spin. The branch to the 6.235 MeV state (11%) indicates spin assignments of $\frac{15}{2}^+$, $\frac{13}{2}^+$, or $\frac{11}{2}^+$ if the 6.235 MeV state is a $\frac{13}{2}^+$ state. The $\frac{15}{2}^+$ assignment is excluded due to the branch to the $\frac{9}{2}^+$ state. If the 6.235 MeV state is a $\frac{9}{2}^+$ state, spins of $\frac{11}{2}^+$, $\frac{9}{2}^+$, or $\frac{7}{2}^+$ are indicated. The branch to the 6.114 MeV state (36%) did not help to restrict the spin of the 7.267 MeV state since the spin of the 6.114 MeV state has not been limited further than $\frac{5}{2}^+$ to $\frac{11}{2}^+$. However, the mixing ratio analysis of this transition was performed for all possible combinations of initial and final spins. The results were not strongly dependent on the spin of the 6.114 MeV state and always allowed only a dipole transition. Therefore, although the spin of neither the 6.114 nor 7.267 MeV states have been uniquely determined, the spin of the 6.114 MeV state is limited to one unit of \hbar more or less than the spin of the 7.267 MeV state. This leads to the following limitations on the spin of the 6.114 MeV state: If the spin of the 6.235 MeV state is $\frac{13}{2}^+$, then the spin of the 6.114 MeV state is $\frac{11}{2}^+$ or $\frac{9}{2}^+$; if the spin of the 6.235 MeV state is $\frac{9}{2}^+$, then the spin of the 6.114 MeV state is $\frac{11}{2}^+$, $\frac{9}{2}^+$, $\frac{7}{2}^+$, or $\frac{5}{2}^+$.

It should be noted that the $^{22}\text{Ne}(^3\text{He}, d)^{23}\text{Na}$ reaction indicates a ($\frac{5}{2}^+$, $\frac{7}{2}^+$) assignment for a state at 7.275 MeV. However, the $^{25}\text{Mg}(d, \alpha)^{23}\text{Na}$ reaction indicates a doublet of states at this excitation energy.²¹ The present 7.267 MeV state is very probably the other member of this doublet.

5. Transitions from the 9.038 MeV state

The transition to the $\frac{11}{2}^+$ state at 5.534 MeV (21%) limited the range of possible spins to be $\frac{7}{2}^+$ to $\frac{15}{2}^+$ with the $\frac{15}{2}^+$ and $\frac{11}{2}^+$ assignments favored at the 23% confidence level ($\chi^2=1.4$). As shown in Fig. 11, the transition to the 6.235 MeV state (60%) indicated a $\frac{15}{2}^+$, $\frac{13}{2}^+$, or $\frac{11}{2}^+$ assignment if the spin of the 6.235 MeV state is a $\frac{13}{2}^+$ state and a $\frac{11}{2}^+$, $\frac{9}{2}^+$, or $\frac{7}{2}^+$ assignment if the 6.235 MeV state is a $\frac{9}{2}^+$ state. The $\frac{13}{2}^+$ ($\frac{9}{2}^+$) assignment is favored at the 40% confidence level ($\chi^2=1.0$) if the spin of the 6.235 MeV state is $\frac{13}{2}^+$ ($\frac{9}{2}^+$). The analysis of the transition to the 7.267 MeV state (19%) excluded a quadrupole transition. However, since the spin of the 7.267 MeV state has only been limited to be $\frac{7}{2}^+$ to $\frac{13}{2}^+$, this result alone does not help to limit the spin of

TABLE VII. Summary of spin sequences indicated by the present data.

E_x (MeV)	Allowed J^π			Allowed J^π	
If 6.235 is	$\frac{9^+}{2}$			$\frac{13^+}{2}$	
and 7.267 is	$\frac{11^+}{2}$	$\frac{9^+}{2}$	$\frac{7^+}{2}$	$\frac{13^+}{2}$	$\frac{11^+}{2}$
then 6.114 is	$\frac{9^+}{2}$	$\frac{11^+}{2}, \frac{7^+}{2}$	$\frac{9^+}{2}, \frac{5^+}{2}$	$\frac{11^+}{2}$	$\frac{9^+}{2}$
9038 is	$\frac{11^+}{2}, \frac{9^+}{2}$	$\frac{11^+}{2}, \frac{9^+}{2}, \frac{7^+}{2}$	$\frac{9^+}{2}, \frac{7^+}{2}$	$\frac{15^+}{2}, \frac{13^+}{2}, \frac{11^+}{2}$	$\frac{13^+}{2}, \frac{11^+}{2}$
9803 is	$\frac{11^+}{2}, \frac{9^+}{2}$	$\frac{11^+}{2}, \frac{9^+}{2}, \frac{7^+}{2}$	$\frac{9^+}{2}, \frac{7^+}{2}$	$\frac{15^+}{2}, \frac{13^+}{2}, \frac{11^+}{2}$	$\frac{13^+}{2}, \frac{11^+}{2}, \frac{9^+}{2}$

the 9.038 MeV state. But if the spin of the 6.235 MeV state is assumed to be either of its two possible values, then the spin of the 7.267 MeV state is further limited, and the spin of the 9.038 MeV state is also limited. The implications of the various possible spin assignments are shown in Table VII. The above assignments are consistent with, and act as further refinements on the findings of Frank *et al.*¹ who analyzed only the transition to the 6.235 MeV state and of Green *et al.*⁴ who analyzed the transitions to the 6.235 and 5.534 MeV states.

6. Transitions from the 9.803 MeV state

The transition to the $\frac{11^+}{2}$ state at 5.534 MeV (20%) limited the range of possible spins to be $\frac{7^+}{2}$ to $\frac{15^+}{2}$. As shown in Fig. 11 the transition to the 6.235 MeV state (51%) indicated a $\frac{9^+}{2}$ to $\frac{15^+}{2}$ assignment if the spin of the 6.235 MeV state is $\frac{13^+}{2}$ and $\frac{5^+}{2}$ to $\frac{11^+}{2}$ assignment if the spin of the 6.235 MeV state is $\frac{9^+}{2}$. The elimination of the $\frac{17^+}{2}$ assignment for the 9.803 MeV state is important since it has been suggested that this state is the $\frac{17^+}{2}$ member of the ground state rotational band.^{3,4,6} For this reason the angular correlation data are explicitly presented in Fig. 8, and as can be seen these data also support the $\frac{15^+}{2}$ assignment.

The analysis of the transition to the 7.267 MeV state (29%) excluded a quadrupole transition. As was the case with the 9.038 MeV state, this further limits the spin of the 9.803 MeV state depending upon the spin of the 6.235 and 7.267 MeV states as shown in Table VII. Once again, these assignments are consistent with the findings of Green *et al.*⁴ who analyzed the transition to the 6.235 MeV state. It is important to note that the 1.153, 1.770, 2.534, and 4.271 MeV γ rays are present in the spectra of Ref. 4, but were not identified due to insufficient resolution or statistics.

7. Transitions from the 11.25, 11.52, and 11.63 MeV states

These states were not populated strongly enough in the present reaction to allow spectroscopic information to be extracted. However, these states do cascade through the 7.267 and 6.235 MeV states since the 4564 and 3533 keV γ rays are present in the γ -ray spectra which are gated on this triplet of states. No γ rays indicating decay through the 9.038 or 9.803 MeV state could be identified.

8. Transition from the 12.591 MeV state

This state was observed to decay to the 7.267 MeV state with a 5324 keV γ ray. In the γ -ray spectrum of Fig. 5, there is a single peak above this γ ray which has been tentatively identified as the first escape peak of a 6355 keV γ ray which would imply a transition to the 6.235 MeV state. In addition, a weak 2792 keV γ ray indicates a branch to the 9.803 MeV state. The high energy shoulder on the 3533 keV γ ray in Fig. 5 would be the corresponding 3569 keV γ ray which deexcites the 9.803 MeV state. An angular correlation analysis was performed on the 5324 keV γ ray which probably includes a second escape peak from the 6355 keV γ ray. No attempt was made to correct for this effect. The angular correlation analysis was carried out assuming that both the 6.235 and 7.267 MeV states are $\frac{13^+}{2}$ states. It indicated spin assignments of $\frac{15^+}{2}$, $\frac{13^+}{2}$, or $\frac{11^+}{2}$ for the 12.591 MeV state. Naturally, if either the 6.235 or the 7.267 MeV states is not a $\frac{13^+}{2}$ state this calculation is invalid.

9. Transitions from states at excitation energies greater than 13.0 MeV

All states above 13 MeV excitation energy decay predominantly by particle emission to states in

^{22}Na , ^{22}Ne , ^{19}F , and ^{19}Ne . It has been suggested that states at 14.24 and 14.70 MeV excitation energy are the $\frac{19}{2}^+$ and $\frac{21}{2}^+$ members of the ground state rotational band.⁶ Particular care was taken to locate evidence of transitions from the 14.5 MeV gate region to the 9.038 and 9.803 MeV states, but none was found.

G. Further discussion of spin assignments

While only spin limits could rigorously be made in the previous section, a large amount of additional experimental evidence indicates that the highest possible spins are the correct ones for the states excited in this reaction. This additional evidence will now be discussed.

Recently, Fletcher *et al.*²³ used the $^{12}\text{C}(^{12}\text{C}, ^8\text{Be})-^{16}\text{O}$ reaction to determine a J^π assignment of 12^+ for a resonantlike structure at $E_{\text{c.m.}}(^{12}\text{C}) = 19.45$ MeV, with $\Gamma_{\text{c.m.}} = 250$ keV. In addition, Cosman *et al.*² have indirectly inferred a J^π assignment of 12^+ for the resonant structure in the $^{12}\text{C}(^{12}\text{C}, p)^{23}\text{Na}$ reaction ($\Gamma_{\text{c.m.}} = 400$ keV) at $E_{\text{c.m.}}(^{12}\text{C}) = 19.30$ MeV which is the subject of the present investigation. In the following it will therefore be assumed that a compound system with J^π of 12^+ is predominantly formed at the present beam energy of $E_{\text{c.m.}}(^{12}\text{C}) = 19.41$ MeV. This is not to imply that only the 12^+ resonance is being excited at $E_{\text{c.m.}}(^{12}\text{C}) = 19.45$ MeV, the presence of the continuum of presumably lower spin states in Fig. 1 testifies to the probable excitation of compound states with $J < 12$.

Transmission coefficients calculated for protons incident on ^{23}Na as shown in Fig. 12 indicate that the grazing $l = 4$ partial waves populate the 9.038 and 9.803 MeV states strongly with the $l = 6$ contributions an order of magnitude less. As an additional check of the validity of excluding $l = 6$ partial waves, penetrability calculations were per-

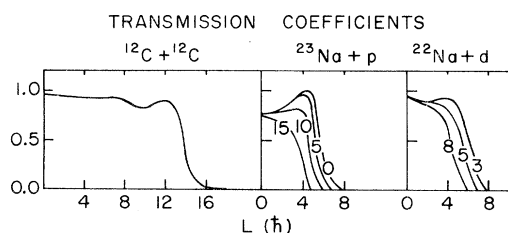


FIG. 12. Transmission coefficients for $^{12}\text{C} + ^{12}\text{C}$, $^{23}\text{Na} + p$, and $^{22}\text{Na} + d$. The ^{12}C elastic scattering transmission coefficient was calculated for 38.8 MeV incident energy. For the proton and deuteron cases, the calculation was performed as a function of the excitation energy (indicated, in MeV, on the curves) of the residual nucleus. Optical model potentials were taken from Refs. 24 and 25.

formed. With an interaction radius of $R = 1.20(A_1^{1/3} + A_2^{1/3})$, the penetrability for the $l = 4$ partial wave to the 9.803 MeV state is a factor of 40 greater than that for $l = 6$. Consequently, the most probable angular momentum is consistent with spins $\geq \frac{15}{2}$ for the two enhanced states in ^{23}Na and also is consistent with spins of $\frac{11}{2}$ or $\frac{13}{2}$ for the more weakly populated states at 5.534, 6.114, 6.235, and 7.267 MeV excitation. As would be expected from this calculation, the $\frac{9}{2}^+$ and $\frac{7}{2}^+$ states at 2.076 and 2.704 MeV excitation energy are populated with small cross sections since they must proceed by $l = 8$ partial waves. Thus, the $J = \frac{15}{2}$ assignments for the 9.038 and 9.803 MeV states are the only ones consistent with all of the information.

As was pointed out in Ref. 26, the $E_x = 4.523$ MeV state in ^{22}Na resonates at nearly the same incident ^{12}C beam energy ($E_B = 38.6$ MeV) as the 9.038, 9.803, and 12.591 MeV states. In our present experiment, we have simultaneously obtained $^{12}\text{C}(^{12}\text{C}, d\gamma)^{22}\text{Na}$ data,²⁷ and the particle- γ analysis confirms the specific population of the 4.52 MeV state. Generally these transitions have been suggested as a $7^+ \rightarrow 5^+ \rightarrow 3^+$ spin sequence by Freeman *et al.*²⁸ and by Spear *et al.*²⁹; however, the latter authors note that the 7^+ is not a rigorous assignment and give $J^\pi = 7^+$ or 5^+ for the 4.52 MeV state from their $^{19}\text{F}(\alpha, n\gamma)^{22}\text{Na}$ neutron- γ correlation studies. If the 4.52 MeV state were a 5_2^+ , then a transition to the 3^+ ground state would be expected. In our data, no 4.523 MeV γ -ray transition to the $J^\pi = 3^+$ ground state is observed, and we limit such a branch to $\leq 1\%$. This limit combines with the reported lifetime of 115_{-35}^{+50} fsec (Ref. 28) and an estimated mixing ratio of $\delta \leq 0.02$ to give an $E2$ transition strength of only 0.01 W.u. for the $5_2^+ \rightarrow 3^+$ sequence. Such retardation is difficult to reconcile with the observed $98 \pm 2\%$ branch to the 1.528 MeV (5^+) state (an $E2$ strength of 3.3 W.u.) and this latter state's enhanced $E2$ transition to the ground state. The 5^- assignment can be excluded by consideration of the strength of the $5^- \rightarrow 5^+$ (4.523 \rightarrow 1.528 MeV) sequence with Spear's mixing ratio which would give $|M2|^2 > 30$ W.u. (Ref. 29). In addition, transmission coefficient calculations show in Fig. 12 that the $l = 4$ partial waves also dominate the deuteron channel for $E_x = 4.5$ MeV in ^{22}Na . Again, with the compound state spin determined as 12, the only possible spin assignment consistent with all the information is $J^\pi = 7^+$ for the $E_x = 4.523$ MeV state.

Analysis of Table VII shows that once a lower spin limit of $\frac{15}{2}$ is placed on the states at 9.0 and 9.8 MeV, these assignments follow: 6.114 MeV state $\frac{11}{2}^+$; 6.235 MeV state $\frac{13}{2}^+$; 7.267 MeV state $\frac{13}{2}^+$; 9.038 MeV state $\frac{15}{2}^+$; and 9.803 MeV state $\frac{15}{2}^+$.

Since the 6.235 and 7.267 MeV states are $\frac{13}{2}^+$ states, the crude angular correlation analysis performed simultaneously on the transitions into these levels from the 12.591 MeV state takes on more meaning, and an $\frac{11}{2}^+$ to $\frac{15}{2}^+$ assignment is indicated for the 12.591 MeV state. Once again, the $\frac{11}{2}^+$ and $\frac{13}{2}^+$ assignments may be excluded since the transmission coefficients describing the appropriate $l=6$ partial wave are essentially zero. As may also be seen in Fig. 12, the transmission coefficients for $l=4$ partial waves leading to the 12.591 MeV state are about 30% less than those $l=4$ partial waves leading to the 9.803 and 9.038 MeV states. This accounts for the relative populations of these states in the present reaction. Following this same procedure, one would predict that the probable $\frac{15}{2}^+$ or $\frac{17}{2}^+$ states at about 11.5 MeV excitation energy would be populated with strength rivaling the 9.803 MeV state. However, it must be remembered that these states are not enhanced at $E_B=38.8$ MeV and it is therefore impossible to draw any conclusions from the relative populations.

The extended decay scheme which results from the present work is shown in Fig. 9. Each state of spin J shown in the figure decays by dipole and quadrupole transitions to states with spins $J-1$ and $J-2$, respectively.

H. Comparison to theory

To test nuclear model calculations, the decay information and spin assignments resulting from the present analysis are compared with three model calculations. The two types of nuclear models having the most success in this mass region are the Nilsson model and the extended shell model. Two Nilsson model calculations are compared with the data. The first Nilsson model calculation was taken from the literature, and was performed by Frank *et al.*¹ The six positive parity bands occurring in the $2s-1d$ shell were included in a band mixing calculation, with the parameters δ , κ , and μ fixed at +0.4, 0.1, and 0.0, respectively. The value of +0.4 for δ is consistent with the measured ground state quadrupole moment of 10 fm^2 . These parameters were chosen in order to reproduce the level structure at excitation energies below 6.0 MeV. The moment of inertia parameter for each band was fixed at 240 keV, but the bandhead energies were treated as adjustable parameters.

The second Nilsson model calculation was performed by Zurmühle.¹⁸ The same six positive parity bands were included in a mixing calculation with δ , κ , and μ fixed at +0.4, 0.08, and 0.0, respectively. The calculation was performed using the results of the present experiment as a basis

for parameter adjustments. In particular, the moment of inertia parameter was decreased to 180 keV in order to depress the energies of the high-spin states in accord with the $\frac{15}{2}^+$ assignments for the states at 9.038 and 9.803 MeV excitation. The strength of this spin orbit coupling was then varied in order to reproduce the level structure of known low-lying positive parity states. Best agreement was found with $\kappa=0.08$. Bandhead energies were not renormalized and δ and μ were fixed at +0.4 and 0.0, respectively.

The last calculation to be discussed is a recent shell-model calculation by Chung and Wildenthal.³⁰ The general features of such calculations have been discussed by Halbert, McGrory, Wildenthal, and Pandya.³¹ This calculation was carried out in the full $d_{5/2}-s_{1/2}-d_{3/2}$ basis space and uses as a Hamiltonian two-body matrix elements obtained by empirically adjusting the matrix elements to best fit low-lying level energies in the $A=18-24$ region.³⁰ The single particle energies are taken from the ^{17}O experimental spectrum.

The level scheme as determined by the present experiment is compared with these shell model

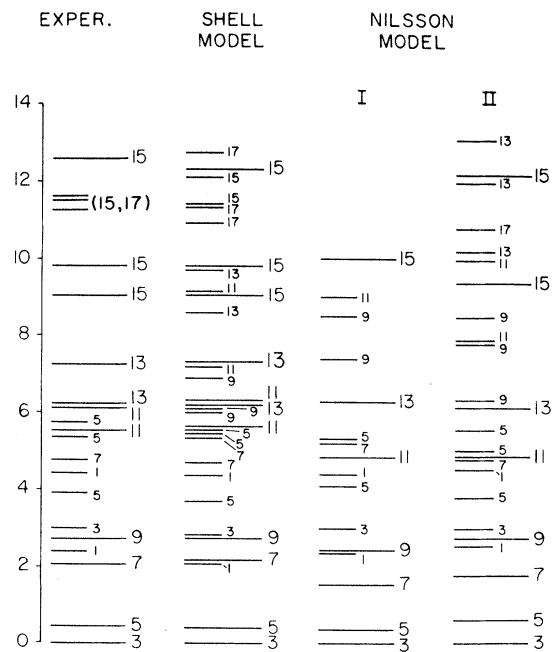


FIG. 13. Level scheme indicated by the present and previous experiments compared with shell-model and Nilsson model calculations. All the known positive parity states below 6.0 MeV are included and are labeled in lower case print. Each state is labeled as $2J$. All predicted levels with energies less than 6.0 MeV are shown. When available, the four lowest-lying states of a given spin are shown for spins greater than $\frac{9}{2}^+$.

predictions in Fig. 13. The shell model reproduces the experimental level scheme remarkably well. The only apparent discrepancy is the inverted order of the $\frac{11}{2}^+$ and $\frac{13}{2}^+$ states at 6.114 and 6.235 MeV excitation energy. Both Nilsson model calculations reproduce the low-lying structure quite well, but fail to predict enough high-spin states at excitation energies above 6.0 MeV. Including higher-lying bandheads into the mixing calculations would not solve this problem, since the associated bandhead energies would lie above 6.0 MeV excitation energy. In order to depress the $\frac{11}{2}^+$ to $\frac{13}{2}^+$ members of these bands to the region of 6 to 10 MeV excitation energy, a smaller moment of inertia would be required and this smaller moment of inertia would make it impossible to reproduce the low-lying energies.

In Tables V, VI, VIII, and IX, the transition

strengths, branching ratios, lifetimes, and mixing ratios calculated from the present experiment are compared to the Nilsson and shell-model predictions. Also included in these tables are the results for the low-lying positive parity states which were not populated with the $^{12}\text{C}(^{12}\text{C}, p)^{23}\text{Na}$ reaction at $E_{\text{c.m.}}(^{12}\text{C}) = 19.41$ MeV.

The shell model predicts the branching ratios to within about 20% for every transition except those from the 2393 and 3916 keV states. All the predicted mean lives and mixing ratios are within two standard deviations of the quoted error of the experimental values except for the mean life of the 2393 \rightarrow 0 keV transition. The theoretical transition strengths are accurate to within the quoted errors for most transitions. The transition strengths which are not accurately predicted are generally slightly overestimated in the theoretical

TABLE VIII. Nilsson model I transition strengths as compared with the experimental values. Experimental transition strengths were obtained using the experimental values of δ , τ , and BR shown in Table VI when the data were available. Theoretical transition strengths are from Ref. 1.

E_i (keV)	J_i	E_f (keV)	J_f	$\Gamma(M1)(\text{W.u.})$			$\Gamma(E2)(\text{W.u.})$	
				Exp.	Theory ^a		Exp.	Theory
440	$\frac{5}{2}^+$	0	$\frac{3}{2}^+$	0.23 ± 0.01	0.13	(0.25)	25.3 ± 3.8	19.0
2076	$\frac{7}{2}^+$	0	$\frac{3}{2}^+$				11.8 ± 2.0	11.0
		440	$\frac{5}{2}^+$	0.16 ± 0.02	0.09	(0.20)	13.9 ± 3.4	15.0
2393	$\frac{1}{2}^+$	0	$\frac{3}{2}^+$	$< 0.002^b$	0.67	(0.07)	$< 2.0^b$	2.9
		440	$\frac{5}{2}^+$				2.9 ± 0.4^b	0.16
2704	$\frac{9}{2}^+$	440	$\frac{5}{2}^+$				20.1 ± 5.5	14.0
		2076	$\frac{7}{2}^+$	0.41 ± 0.11	0.34	(0.48)	44.0 ± 25.0	5.0
2984	$\frac{3}{2}^+$	0	$\frac{3}{2}^+$	0.14 ± 0.02	0.24	(0.007)	0.01 ± 0.04	0.05
		440	$\frac{5}{2}^+$	0.16 ± 0.03	1.01	(0.08)	1.30 ± 0.91	1.1
3916	$\frac{5}{2}^+$	0	$\frac{3}{2}^+$	0.04 ± 0.01	0.05	(0.0015)	0.85 ± 0.29	0.46
		440	$\frac{5}{2}^+$	$< 0.007^b$	0.12	(0.004)	$< 3.3^b$	0.84
4430	$\frac{1}{2}^+$	0	$\frac{3}{2}^+$	$< 1.4^b$	0.67	(0.67)	$< 400^b$	1.8
		2393	$\frac{1}{2}^+$	1.2 ± 0.3^b				
4775	$\frac{7}{2}^+$	440	$\frac{5}{2}^+$	0.11 ± 0.06	0.033	(0.011)	1.13 ± 0.63	0.04
		2076	$\frac{7}{2}^+$	0.22 ± 0.11	0.21	(0.000 15)	0.31 ± 1.60	0.08
		2704	$\frac{9}{2}^+$					
5374	$\frac{5}{2}^+$	0	$\frac{3}{2}^+$	0.07 ± 0.04	0.40	(0.13)	0.04 ± 0.05	0.9
		440	$\frac{5}{2}^+$	0.39 ± 0.21	0.024	(0.08)	7.75 ± 5.08	2.0
		2076	$\frac{7}{2}^+$	0.62 ± 0.34	0.47	(0.38)	8.44 ± 10.10	0.5
		2984	$\frac{3}{2}^+$					
5534	$\frac{11}{2}^+$	2076	$\frac{7}{2}^+$				7.7 ± 4.1	18.0
		2704	$\frac{9}{2}^+$	0.071 ± 0.036	0.12	(0.22)	1.68 ± 1.04	6.0

TABLE VIII. (Continued)

E_i (keV)	J_i	E_f (keV)	J_f	$\Gamma(M1)$ (W.u.)		$\Gamma(E2)$ (W.u.)	
				Exp.	Theory ^a	Exp.	Theory
6114	$\frac{11}{2}^+$	2076	$\frac{7}{2}^+$		No available		
		2704	$\frac{9}{2}^+$		state		
6235	$\frac{13}{2}^+$	2704	$\frac{9}{2}^+$			15.0 ± 6.9	17.0
		5534	$\frac{11}{2}^+$	0.45 ± 0.29	0.45 (0.58)	118 ± 201	2.0
7267	$\frac{13}{2}^+$	2704	$\frac{9}{2}^+$		no		
		5534	$\frac{11}{2}^+$		available		
		6235	$\frac{13}{2}^+$		state		
		6114	$\frac{11}{2}^+$				
9038	$\frac{15}{2}^+$	5534	$\frac{11}{2}^+$		no		
		6235	$\frac{13}{2}^+$	0.057 ± 0.027	available	0.043 ± 0.144	
		7267	$\frac{13}{2}^+$		state		
9804	$\frac{15}{2}^+$	5534	$\frac{11}{2}^+$				
		6235	$\frac{13}{2}^+$	0.030 ± 0.014	0.13 (0.22)	1.20 ± 1.02	3.0
		6114	$\frac{11}{2}^+$				
		7267	$\frac{13}{2}^+$				

^a The $\Gamma(M1)$ values were modified to take into account effects of isospin. These modified values of $\Gamma(M1)$ are in (parentheses).

^b These experimental values were obtained from Ref. 1.

TABLE IX. Nilsson model predictions of mean lifetimes, mixing ratios, and branching ratios as compared with experimental values. Theoretical values of τ , BR, and δ were obtained from Ref. 32.

E_i (keV)	J_i	E_f (keV)	J_f	Mixing ratio		Mean life (fsec)		Branching ratio (%)	
				Exp.	Theory	Exp.	Theory	Exp.	Theory
440 ^a	$\frac{5}{2}^+$	0	$\frac{3}{2}^+$	-0.057 ± 0.004	-0.07	1600 ± 80	2100	100	100.0
2076 ^a	$\frac{7}{2}^+$	0	$\frac{3}{2}^+$	+0.14 ± 0.11	0	40 ± 15	44	9 ± 1	9.0
		440	$\frac{5}{2}^+$	-0.19 ± 0.02	-0.22			91 ± 1	91.0
2393 ^b	$\frac{1}{2}^+$	0	$\frac{3}{2}^+$		+0.04	800 ± 200	2	65 ± 1	100.1
		440	$\frac{5}{2}^+$		0			35 ± 1	0.0
2704 ^a	$\frac{9}{2}^+$	440	$\frac{5}{2}^+$	+0.00 ± 0.03	0	110 ± 30	150	64 ± 1	60.0
		2076	$\frac{7}{2}^+$	-0.08 ± 0.02	-0.04			36 ± 1	40.0
2984 ^b	$\frac{3}{2}^+$	0	$\frac{3}{2}^+$	+0.01 ± 0.02	-0.006	5 ± 1	1	58 ± 1	35.0
		440	$\frac{5}{2}^+$	+0.09 ± 0.03	-0.03			42 ± 1	65.0
3916 ^b	$\frac{5}{2}^+$	0	$\frac{3}{2}^+$	-0.22 ± 0.03	+0.31	10 ± 2	2.0	82 ± 2	12.0
		440	$\frac{5}{2}^+$		+0.12			8 ± 2	59.0
4430 ^b	$\frac{1}{2}^+$	0	$\frac{3}{2}^+$		0	0.27 ± 0.03	0.4	94 ± 2	96.0
		2393	$\frac{1}{2}^+$		0			6 ± 2	4.0
4775 ^b	$\frac{7}{2}^+$	440	$\frac{5}{2}^+$	-0.17 ± 0.02	-0.02	< 2	2.0	60 ± 3	18.0
		2076	$\frac{7}{2}^+$	+0.04 ± 0.10	-0.02			27 ± 2	37.0
		2704	$\frac{9}{2}^+$		-0.02			13 ± 2	45.0

TABLE IX. (Continued)

E_i (keV)	J_i	E_f (keV)	J_f	Mixing ratio		Mean life (fsec)		Branching ratio (%)	
				Exp.	Theory	Exp.	Theory	Exp.	Theory
5374 ^c	$\frac{5}{2}^+$	0	$\frac{3}{2}^+$	$+0.05 \pm 0.05$	-0.02	~ 0.37	0.6	13 ± 1	87.0
		440	$\frac{5}{2}^+$	$+0.27 \pm 0.05$	-0.02			60 ± 3	7.0
		2076	$\frac{7}{2}^+$	-0.15 ± 0.08	+0.02			27 ± 3	6.0
		2984	$\frac{3}{2}^+$						0.0
5534 ^a	$\frac{11}{2}^+$	2076	$\frac{7}{2}^+$	$+0.08 \pm 0.25$	0	14 ± 7	6.0	26 ± 5	27.0
		2704	$\frac{9}{2}^+$	-0.17 ± 0.03	-0.25			74 ± 5	73.0
6114 ^a	$\frac{11}{2}^+$	2076	$\frac{7}{2}^+$			50 ± 11		17 ± 4	
		2704	$\frac{9}{2}^+$	$-0.26^{+0.26}_{-0.41}$				83 ± 4	
6235 ^a	$\frac{13}{2}^+$	2704	$\frac{9}{2}^+$	$+0.09 \pm 0.5$	0	22 ± 10	20.0	89 ± 5	91.0
		5534	$\frac{11}{2}^+$	-0.14 ± 0.11	-0.03			11 ± 5	9.0
7267 ^a	$\frac{13}{2}^+$	2704	$\frac{9}{2}^+$	$+0.03 \pm 0.24$		26 ± 8		53 ± 5	
		5534	$\frac{11}{2}^+$						
		6235	$\frac{13}{2}^+$	$+0.57^{+3.63}_{-0.74}$				11 ± 2	
		6114	$\frac{11}{2}^+$	-0.01 ± 0.09				36 ± 3	
9038 ^a	$\frac{15}{2}^+$	5534	$\frac{11}{2}^+$			No predictions available			
		6235	$\frac{13}{2}^+$						
		7267	$\frac{13}{2}^+$						
9803 ^a	$\frac{15}{2}^+$	5534	$\frac{11}{2}^+$			No predictions available			
		6235	$\frac{13}{2}^+$						
		6114	$\frac{11}{2}^+$						
		7267	$\frac{13}{2}^+$						

^a Experimental values of τ , BR, and δ were obtained from Tables I, III, and IV.

^b Experimental values of τ , BR, and δ were obtained from Ref. 9.

^c Experimental values of τ , BR, and δ were obtained from Ref. 32.

calculations. Overall, the shell model does an excellent job of reproducing the spectroscopic properties of ^{23}Na .

V. CONCLUSIONS

The $^{12}\text{C}(^{12}\text{C}, p)^{23}\text{Na}$ reaction has proven to be extremely useful in studying high-spin states in ^{23}Na . The general applicability of "heavy ion—light ion out" particle- γ -ray coincidence measurements as a spectroscopic tool for investigating high-spin states is probably limited since most of these reactions are typified by microbarn cross sections. However, if an enhanced cross section can be found for even one state the stringent alignment conditions imposed on the residual nucleus allow particle- γ -ray angular correlations to be performed on transitions from states which are included in the γ -ray cascade from that state. The resulting measurements produce decay information and spin limitations on the states which

participate in this cascade.

Using the particle- γ -ray angular correlation technique, a number of high-spin states were identified in ^{23}Na , and their decay properties were studied. A comparison of the results of these measurements with shell and Nilsson model predictions indicate that the current highly sophisticated shell-model calculations provide an excellent description of the decay properties of ^{23}Na up to 13.0 MeV excitation energy. The Nilsson model calculations were not able to compete with the shell-model calculations because of the restricted basis of states which were employed. If these calculations were expanded to take into account the breaking of neutron and proton pairs with variation of the deformation and moment of inertia parameters the Nilsson model could possibly give much better results. Of course, such complex modifications would eliminate the appealing simplicity of the Nilsson model.

The authors wish to acknowledge Dr. B. H. Wildenthal and Dr. W. Chung for graciously making their latest shell-model calculations available, Dr. R. W. Zurmühle for making his Nilsson model calculations available and for his valuable comments concerning their applicability, Dr. R. V. LeClaire for his computer programming assistance, Dr. Henri van Rinsvelt for allowing us

to use his Ge(Li) detector and for helping to collect the data, Dr. A. F. Zeller, Dr. G. R. Morgan, and Dr. R. J. Puigh for helping to collect the data, and the members of the Florida State University tandem operations group, electronics shop, and machine shop for their help in the developmental stages of this experiment.

*Work supported in part by the National Science Foundation under Grants Nos. NSF-PHY-75-3767-A01, NSF-GU-2612, and NSF-GJ-367.

†Present address: Lawrence Berkeley Laboratory, University of California, Berkeley, California 94720.

- ¹G. G. Frank, R. V. Elliott, R. H. Spear, and J. A. Kuehner, *Can. J. Phys.* **51**, 1155 (1973).
²K. Van Bibber, E. R. Cosman, A. Sperduto, T. M. Cormier, and T. N. Chin, *Phys. Rev. Lett.* **32**, 687 (1974); E. R. Cosman, T. M. Cormier, K. Van Bibber, A. Sperduto, G. Young, J. Erskine, L. R. Greenwood, and O. Hansen, *ibid.* **35**, 265 (1975).
³T. M. Cormier, E. R. Cosman, L. Grodzins, O. Hansen, S. Steadman, K. Van Bibber, and G. Young, in *Proceedings of the International Conference on Reactions Between Complex Nuclei, Nashville, Tennessee, 1974*, edited by R. L. Robinson, F. K. McGowan, J. B. Ball, and J. H. Hamilton (North-Holland, Amsterdam/American Elsevier, New York, 1974), p. 343.
⁴P. W. Green, G. D. Jones, D. T. Kelly, J. A. Kuehner, and D. T. Petty, *Phys. Rev. C* **12**, 887 (1975); B. Back, R. Betts, C. Gaarde, and H. Oeschler, *ibid.* **13**, 875 (1976).
⁵G. J. KeKelis, A. H. Lumpkin, and J. D. Fox, *Phys. Rev. Lett.* **35**, 710 (1975); G. J. KeKelis, Ph.D. dissertation, Florida State University, 1975 (unpublished).
⁶J. G. del Campo, D. E. Gustafson, R. L. Robinson, P. H. Stelson, P. D. Miller, J. K. Bair, and J. B. McGrory, *Phys. Rev. C* **12**, 1247 (1975).
⁷D. E. Gustafson, S. T. Thornton, T. C. Schweizer, J. L. C. Ford, Jr., P. D. Miller, R. L. Robinson, and P. H. Stelson, *Phys. Rev. C* **13**, 691 (1976).
⁸K. R. Chapman, *Nucl. Instrum. Methods* **124**, 299 (1975).
⁹P. M. Endt and C. van der Leun, *Nucl. Phys.* **A214**, 1 (1973).
¹⁰A. C. L. Barnard, J. B. Swint, and T. B. Clegg, *Nucl. Phys.* **86**, 130 (1966).
¹¹A. E. Litherland and A. J. Ferguson, *Can. J. Phys.* **39**, 788 (1961).
¹²T. Yamazaki, *Nucl. Data* **A3**, 1 (1967).
¹³H. J. Rose and D. M. Brink, *Rev. Mod. Phys.* **39**, 306 (1967).

- ¹⁴A. E. Blaugrund, *Nucl. Phys.* **88**, 501 (1966).
¹⁵J. Lindhard, M. Scharff, and H. E. Schiott, K. Dan. Vidensk. Selsk. Mat.-Fys. Medd. **33**, No. 14 (1963).
¹⁶J. Lindhard, Nuclear Science Series, Report No. 39, Publication No. 1133, 1964 (unpublished), p. 1.
¹⁷L. Northcliffe and R. Schilling, *Nucl. Data* **A7**, 233 (1970).
¹⁸R. W. Zurmühle, University of Pennsylvania (private communication).
¹⁹P. M. Endt and C. van der Leun, *Nucl. Data* **A13**, 67 (1974).
²⁰R. A. Lindgren, R. G. Hirko, J. G. Pronko, A. J. Howard, M. W. Sachs, and D. A. Bromley, *Nucl. Phys.* **A180**, 1 (1972).
²¹J. R. Powers, H. T. Fortune, R. Middleton, and O. Hansen, *Phys. Rev. C* **4**, 2030 (1971).
²²J. R. Powers, Ph.D. dissertation, University of Pennsylvania, 1970 (unpublished).
²³N. R. Fletcher, J. D. Fox, G. J. KeKelis, G. R. Morgan, and G. A. Norton, *Phys. Rev. C* **13**, 1173 (1976).
²⁴W. Reilly, R. Wieland, A. Gobbi, M. W. Sachs and D. A. Bromley, *Nuovo Cimento* **13A**, 897 (1973).
²⁵C. M. Perey and F. G. Perey, *Nucl. Data* **A10**, 539 (1972).
²⁶G. J. KeKelis and J. D. Fox, *Phys. Rev. C* **10**, 2613 (1974).
²⁷A. H. Lumpkin, G. J. KeKelis, J. D. Fox, and K. W. Kemper, *Phys. Rev. C* (to be published).
²⁸R. M. Freeman, F. Haas, B. Heusch, J. Fernandez Castillo, J. W. Olness, and A. Gallmann, *Phys. Rev. C* **8**, 2182 (1973).
²⁹R. H. Spear, R. A. I. Bell, M. T. Esat, P. R. Gardner, D. C. Kean, and A. M. Baxter, *Phys. Rev. C* **11**, 742 (1975).
³⁰B. H. Wildenthal and W. Chung, Michigan State University (private communication).
³¹E. G. Halbert, J. B. McGrory, B. H. Wildenthal, and S. P. Pandya, in *Advances in Nuclear Physics*, edited by M. Baranger and E. Vogt (Plenum, New York, 1969), Vol. 3.
³²B. Hass and P. Taras, *Can. J. Phys.* **52**, 49 (1974).